Current Opinion in Solid State and Materials Science 43 (2026) 101288

Contents lists available at ScienceDirect

Current Opinion in Solid State & Materials Science

journal homepage: www.elsevier.com/locate/cossms

Advances in flexible thermal Interface materials with low contact thermal resistance

Yan Zhang [a,1], Xin Dai [a,1], Zikang Liang [a], Ming He [b,c], Yucan Peng [a,*]

[a] Department of Energy and Resources Engineering, School of Mechanics and Engineering Science, Peking University, Beijing 100871, China
[b] Beijing Advanced Innovation Center for Integrated Circuits, School of Integrated Circuits, Peking University, Beijing, China
[c] Frontiers Science Center for Nano-optoelectronics, Peking University, Beijing, China

ARTICLE INFO

Keywords:
Thermal interface materials
Contact thermal resistance
Composite materials

ABSTRACT

Rising power density and device integration have made interfacial heat dissipation a major challenge in thermal management. Thermal interface materials (TIMs) bridge heat sources and sinks, but their practical performance depends on effective thermal resistance rather than thermal conductivity alone. This review focuses on flexible TIMs with low contact thermal resistance and examines how material composition, interfacial interactions, and structural design jointly regulate bulk thermal resistance, bond-line thickness (BLT), and contact thermal resistance (R_C). We examine the physical origins of R_C and summarize recent strategies based on compliant matrices, interfacial adhesion and wetting, adaptive gap filling, continuous thermal networks, and compressible structures. These studies show that increasing thermal conductivity alone can be ineffective when increased modulus, viscosity, or BLT limits interfacial conformability. We conclude that future TIM development should prioritize the coordinated optimization of thermal pathways, interfacial adaptability, BLT, mechanical reliability, and scalable processing under practical conditions.

1. Introduction

The rapid evolution of electronic systems toward higher power density, miniaturization, and multifunctional integration has made heat dissipation a primary constraint on device performance and reliability [1–8]. In highly integrated electronic packages, heat typically traverses multiple solid–solid interfaces before reaching a heat sink or cooling structure [9,10]. Even after precision polishing, these interfaces are not perfectly smooth; they retain micro- and nanoscale roughness, so the real contact area is much smaller than the apparent contact area, and the intervening regions are filled with low-thermal-conductivity air gaps [11,12]. Moreover, dissimilar materials often exhibit different phonon spectra, electron-transport properties, and interfacial bonding states, which cause heat-carrier scattering and introduce Kapitza-type interfacial thermal resistance [11,12]. Thermal interface materials (TIMs) therefore act as gap fillers and heat-transfer media that displace air, increase the real contact area, and create stable heat-transfer pathways between the heat source and the heat sink.

In TIM applications, the total thermal resistance can be simplified as the sum of the bulk thermal resistance of the TIM and the overall contact resistance at the interfaces, which can be expressed as Eq. (1):

$$R_{total} = R_{TIM} + R_C = BLT/k_{TIM} + R_C \quad (1)$$

Here, R_{total} denotes the total thermal resistance of the thermal path, R_{TIM} represents the bulk thermal resistance of the TIM, R_C is the sum of the contact resistances at the heat source to TIM interface and the TIM to heat sink interface, BLT is the bond-line thickness, and k_{TIM} is the effective thermal conductivity of the TIM. This decomposition indicates that lowering R_{total} requires the simultaneous improvement of three variables: increasing k_{TIM}, reducing bond-line thickness (BLT), and decreasing the overall contact resistance R_C. High thermal conductivity remains an important target in TIM design, but it cannot alone represent device-level cooling performance. When k_{TIM} is low, improving bulk thermal conductivity is often the dominant issue. Once the bulk resistance has been reduced by high filler loading, aligned networks, or metallic phases, interfacial conformity, wetting, real contact area, and BLT can become the key factors limiting any further decrease in total

* Corresponding author.
E-mail address: yucan.peng@pku.edu.cn (Y. Peng).
[1] These authors contributed equally

https://doi.org/10.1016/j.cossms.2026.101288
Received 21 May 2026; Received in revised form 19 July 2026; Accepted 22 July 2026
Available online 3 August 2026
1359-0286/© 2026 Elsevier Ltd. All rights are reserved, including those for text and data mining, AI training, and similar technologies.

thermal resistance.

In highly filled polymer TIMs, filler networks help improve k_{TIM}, yet excessive filler loading may reduce flexibility, impair gap-filling capability, and increase the thermal resistance at filler-matrix or TIM-substrate interfaces [13–15]. This framework explains why many high-k TIMs do not always outperform lower-k but more compliant materials in practical packages. Increasing filler content can strengthen heat-transfer pathways and reduce bulk resistance, but it can also raise modulus, yield stress, and BLT, thereby reducing conformability to rough surfaces and increasing contact resistance.

This effective-resistance-centered design logic is especially important for flexible TIMs. A compliant polymer matrix can fill multiscale surface asperities through compression, chain relaxation, and local flow, thereby increasing real contact area and reducing R_C [16–19]. Because most flexible polymers have intrinsically low thermal conductivity, conductive fillers and structured thermal pathways are commonly introduced to lower bulk resistance, including ceramic-filler systems [15,20–22], carbon-based networks [23–25], phase-change-assisted skeletons [26,27], and liquid-metal-mediated thermal bridges. However, higher filler loading or more rigid thermal networks can increase modulus, viscosity, yield stress, and BLT, which weakens wetting, leaves residual micro-voids, and raises contact resistance [12,15,28]. To balance these coupled factors, recent studies have developed compliant polymer architectures [15–17,29], strategies for regulating filler interfaces and molecular adhesion [20,22,30–32], self-adhesive or dynamically reconfigurable interfaces [33–36], and compressible structural designs that enhance real contact area [37–41]. These advances indicate that flexible TIMs require coordinated regulation of matrix compliance, thermal-network continuity, interfacial adhesion, BLT reduction, and long-term mechanical stability. Consequently, the key descriptors for flexible TIMs include not only k_{TIM}, but also compressive modulus, yield stress, rheological behavior, adhesion, wettability, BLT, real contact area, and thermomechanical cycling stability [12,42,43]. These variables jointly determine whether a material can maintain a low effective thermal resistance (R_{EFF}) under pressure, temperature variation, and service-induced perturbations.

Although contact thermal resistance has been interpreted through phonon mismatch, diffuse mismatch, and rough-surface contact mechanics that consider elastic or plastic deformation, these frameworks have not been integrated into a review that connects material selection, interfacial engineering, and structural design [11,12,28]. Existing reviews typically organize TIMs by material class, filler type, or fabrication method. Examples include polymer composites, phase-change materials (PCMs), greases/gels, liquid metals, and carbon-based networks [44,45]. That organization clarifies material development but can obscure common low-contact-resistance mechanisms across different systems. Approaches such as flexible polymer matrices, self-adhesive interfaces, phase-change softening, grease/gel gap filling, liquid-metal wetting, continuous thermal networks, and compressible structures all pursue the same goals: preserve heat-transfer pathways, improve interfacial filling, reduce bond-line thickness, enlarge real contact area, and maintain low-resistance contact during service.

This review examines the synergistic regulation of materials, interfaces, and structures in flexible TIMs aimed at minimizing contact thermal resistance. It begins with the formation mechanism of thermal contact resistance (TCR), evaluation methods, and key parameters such as BLT, pressure, rheology, and reliability. Next, it categorizes three principal design strategies for reducing contact resistance. The first strategy focuses on compliant and adaptive TIMs, where polymer-matrix engineering, self-adhesion, and dynamic reconstruction enhance conformity to rough surfaces. The second addresses gap-filling TIMs for low thermal resistance, where phase-change softening, grease/gel rheology, and liquid-metal wetting produce thin, continuous interfaces with few voids. The third covers structured TIMs for low contact thermal resistance, where continuous thermal networks, compressible architectures, micro-bulges, and deformable terminals link high-conductivity pathways to heat-source and heat-sink surfaces. Framing recent advances around effective thermal resistance, the review stresses that high k_{TIM}, low BLT, low R_C, and long-term interfacial stability must be engineered in concert. Overall, the field is shifting from isolated enhancement of thermal conductivity toward integrated optimization of material compliance, interfacial contact, and structured heat-transfer pathways.

2. Formation of contact thermal resistance

Contact resistance research originates from a macroscopic perspective. When two rough solids contact in ambient air, interfacial heat transfer occurs via three parallel paths, decomposing the total thermal contact conductance into solid spot (h_s), gas (h_g), and radiation (h_r) components:

$$h_{total} = h_s + h_g + h_r \tag{2}$$

Here, h_s denotes conduction through actual micro-asperity contacts, h_g represents conduction via trapped gas molecules in interstitial gaps, and h_r accounts for radiative transfer across gaps. In thermal radiation theory, near-field radiative effects become significant only when the interfacial separation (d) is much smaller than the characteristic wavelength. If the separation is comparable to or larger than the wavelength, it degenerates to ordinary far-field radiation. Since actual engineering surface roughness is mostly on the micrometer scale, the separation is unlikely to be much smaller than the characteristic wavelength (e.g., approximately 3–10 μm at 300–1000 K) [46,47]. Therefore, near-field thermal radiation effects are not significant; only far-field radiation needs to be considered, and its value remains small. The thermal conductivity of the interstitial gas is very low (e.g., approximately 0.026 W m^{-1} K^{-1} for air at room temperature), which is the fundamental reason why thermal interface materials (TIMs) need to fill the micro-gaps to reduce the contact thermal resistance. As illustrated in Fig. 1, direct contact (Fig. 1a) results in limited solid contact spots, whereas TIM insertion (Fig. 1b) effectively bridges the gap.

In TIM applications, the total thermal resistance can be simplified as the sum of the bulk thermal resistance of the TIM and the overall contact resistance at the interfaces, which can be expressed as Eq. (1). In practical optimization, the relative importance of R_{TIM} and R_C changes dynamically with operating conditions. When the thermal conductivity of the TIM is low, improving k_{TIM} (i.e., reducing the bulk thermal resistance) is the primary bottleneck to lowering the total thermal resistance [28,48,49]. However, with the introduction of high-k fillers (e.g., diamond [10,50], boron nitride [51], boron arsenide [52,53], carbon nanotubes [54–56], liquid metal [57]), the bulk thermal resistance decreases significantly. In such cases, the contact thermal resistance R_C, which is limited by surface roughness [58], gap filling ability [59,60], and interfacial phonon mismatch [61,62], becomes the key bottleneck restricting heat dissipation. To date, a large body of work has focused on enhancing k_{TIM} by constructing thermal conduction pathways. A typical strategy is tailoring the 1D/2D orientation of fillers to form percolation networks. However, many of these strategies and processing methods come with a hidden cost when increasing bulk thermal conductivity: high filler loading often leads to a drastic increase in TIM modulus and a decrease in interfacial conformability, thereby worsening the contact thermal resistance [63–65].

In fact, high bulk thermal conductivity and low contact thermal resistance are not necessarily conflicting objectives but require

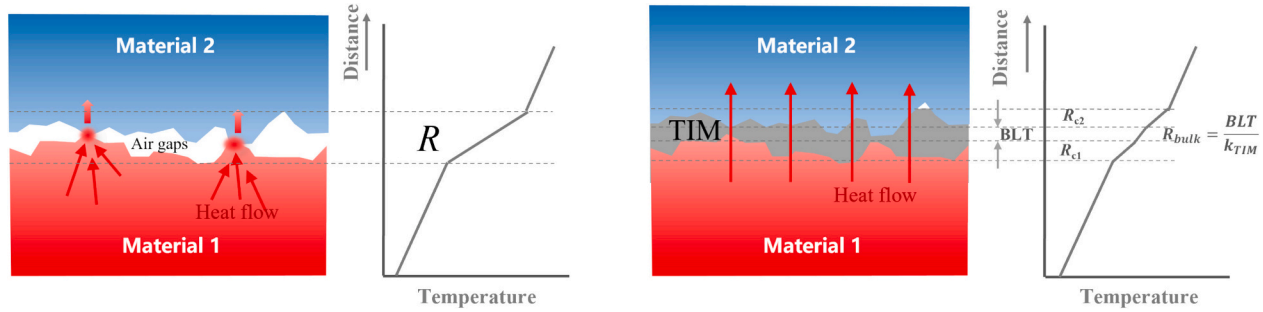

Fig. 1. Schematic of thermal contact resistance between two solid surfaces without and with a thermal interface material (TIM). Without TIM, only a few discrete contact points exist, and air gaps dominate the interface, leading to a large temperature drop. With TIM, the gaps are filled, but two additional interfacial resistances (R_{C1} and R_{C2}) and the bulk resistance of TIM ($R_{TIM} = BLT/k_{TIM}$) are introduced.

synergistic optimization. Contact thermal resistance is essentially a response that depends on operating conditions, governed jointly by contact pressure, surface roughness, viscoelastic state, and interfacial wettability. For example, Xie et al. employed liquid metal to modify the Al_2O_3 surface, significantly improving wettability with a copper substrate and lowering the contact thermal resistance by 65% [65]. Wu et al. designed a poly(urethane-urea-imide) (PUUI)-based dynamic adhesive TIM that achieves adaptive interfacial contact through hydrogen bonding and reversible disulfide exchange, resulting in low thermal contact resistance under zero pressure [35]. These examples prove that through materials chemistry design and microstructural engineering, it is entirely possible to endow a material with excellent interfacial adaptability while maintaining high bulk thermal conductivity. This is precisely the focus of the following sections of this review. Subsequent sections discuss how sophisticated design strategies can break the performance trade-off between the bulk and the interface, thereby achieving truly efficient TIMs.

At the matrix and composite level, we look beyond the contribution of microstructure to bulk thermal conductivity and emphasize its decisive influence on interfacial contact behavior. This includes utilizing ultra-soft polymers with dangling chains as flexible matrices (Fig. 2a), and implementing efficient filler packing (Fig. 2b). While the latter primarily aims to construct conductive pathways, its regulation of the composite's overall flexibility and fatigue resistance is equally critical for enhancing interfacial gap filling and minimizing contact resistance. At the interfacial engineering level, we address the bottlenecks of solid to solid heat transport. Surface energy matching significantly improves stress transfer efficiency and wettability between fillers and the polymer matrix, thereby reducing internal defects (Fig. 3c). Meanwhile, enhanced interfacial adhesion strengthens the interaction between the polymer and heat source/sink surfaces, effectively reducing contact resistance (Fig. 3d). In addition, incorporating phase-change filling (Fig. 3e) and liquid-metal-mediated full contact (Fig. 3f) leverages post-melting fluidity to actively eliminate interfacial voids, achieving a fundamental breakthrough in the interfacial heat transport performance of TIMs.

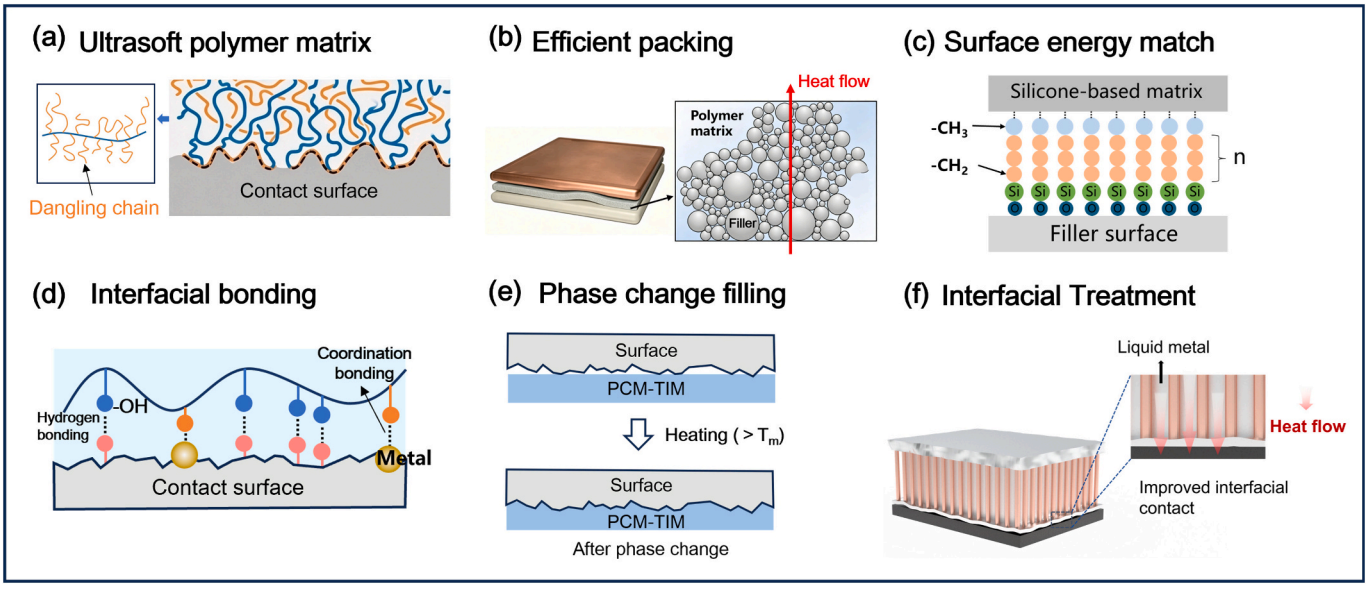

Fig. 2. Schematic illustration of strategies for reducing R_C in TIMs. (a) Ultrasoft polymer matrix: The polymers with dangling chains at the contact surface enhance interfacial compliance. (b) Efficient packing: rational filler packing not only facilitates the formation of continuous thermal conduction pathways but also enables TIMs that are soft, tough, and fatigue-resistant. (c) Surface-energy matching: chemical functionalization (e.g., -CH_2- groups) aligns filler and polymer matrix surface energies for better wetting. Good filler-matrix compatibility enables tunable yield stress in the composite, thereby facilitating low-contact-resistance TIMs. (d) Interfacial bonding: hydrogen bonding and metal complexation strengthen polymer matrix and adhesion to heat-source and heat-sink surfaces. (e) Phase-change filling: phase-change-material (PCM)-based TIM fills gaps upon heating (above T_m) to reduce R_C. (f) Interfacial treatment: liquid metal (LM)-mediated full contact eliminates interfacial gaps, enabling low R_C.

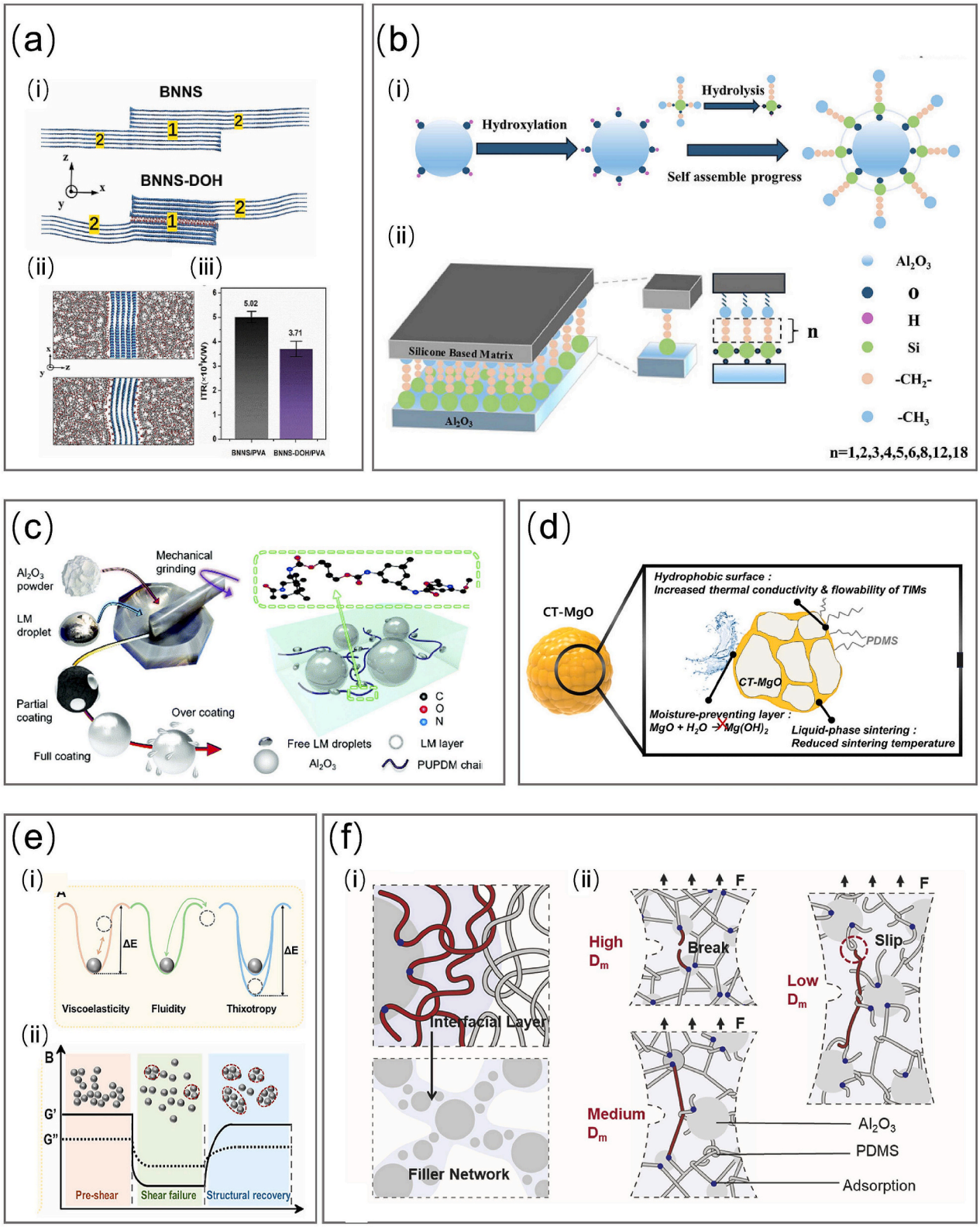

Fig. 3. Interfacial, rheological, and structural strategies for flexible polymer-based TIMs. (a) Interfacial engineering of boron nitride nanosheets: (i) BNNS/BNNS and 1-dodecanol-functionalized BNNS (BNNS-DOH)/BNNS-DOH interface models; (ii) BNNS/PVA and BNNS-DOH/PVA interface models; and (iii) the corresponding interfacial thermal resistances [20]. (b) Surface-energy regulation of Al_2O_3 fillers: (i) preparation of self-assembled monolayer-modified Al_2O_3; and (ii) regulation of filler–matrix compatibility by varying the alkyl-chain length [12]. (c) Liquid-metal-mediated filler design: (i) preparation of core–shell liquid metal/Al_2O_3 fillers; and (ii) incorporation of the hybrid fillers into a PUPDM matrix [22]. (d) CT-MgO fillers designed to improve compatibility with the PDMS matrix and the rheological properties of the composite [31]. (e) Thixotropic behavior of PDMS/AlN composite fluids: (i) energy-landscape representation of viscoelasticity, fluidity, and thixotropy; and (ii) reversible breakdown and reconstruction of the filler network under shear [64]. (f) Fractal-network design of Al_2O_3/PDMS composites: (i) polymer adsorption and entanglement around the filler network; and (ii) stress redistribution in filler networks with different fractal dimensions [63].

3. Interface filling theory: classical models and developments

The physical origin of TCR lies in the non-ideal contact between rough surfaces. To provide theoretical guidance for materials design and performance optimization of TIM, two fundamental questions must first be addressed: How can real contact surfaces be described? How do the size and number of contact spots evolve with applied pressure? Although the classical models developed around these questions vary in form, they collectively point to a set of core physical parameters that govern interfacial heat transfer efficiency—surface topography, material hardness, elastic modulus, and their coupling with contact pressure. These parameters constitute the theoretical basis for material design. This section focuses on the milestone models, aiming to extract from theory the physical principles that can guide materials development.

3.1. Ideal single-spot constriction model

Kottler pioneered the analogy of electrical constriction resistance to thermal problems. Assuming a hyperbolic distribution of heat flow lines, he derived the thermal constriction resistance for an ideal single-spot contact:

$$R_c = \frac{1}{2ka} \tag{3}$$

where k is the thermal conductivity of the material and a is the radius of the contact spot. When two solid surfaces are pressed together, real contact occurs only at the tips of a few asperities. Extending this to multi-spot contact, heat flow converges from the bulk of one solid into the contact spots and then diverges into the other solid, with the former giving rise to constriction resistance and the latter to spreading resistance. Together, they constitute the total thermal resistance of multi-spot contact [47,66]:

$$R_{total} = \frac{1}{4ak_1} + \frac{1}{4ak_2} = \frac{1}{2ak_h} \tag{4}$$

where k_1 and k_2 are the thermal conductivities of the two solids, and $k_h = 2k_1k_2/(k_1 + k_2)$ is the harmonic mean thermal conductivity. The limitation of this model is evident—it fails to capture the random multi-scale characteristics of rough surfaces.

The transition from single-asperity to rough-surface analysis was achieved by Greenwood and Williamson [67,68]. They pointed out that engineering surfaces are populated by numerous asperities with heights obeying a Gaussian distribution, and introduced statistical descriptors for asperity height, curvature radius, and areal density. Based on this statistical framework, subsequent researchers have developed numerous models for solid contact thermal conductance. While varying in form and assumptions, these models converge on a set of key parameters that govern interfacial heat transfer efficiency.

3.2. Classical Cooper-Mikic-Yovanovich (CMY) model and its extensions

Among the numerous models developed subsequently, the CMY model proposed by Cooper, Mikic, and Yovanovich in 1969 stands as the most representative [69]. The model is built on three key assumptions—(a) asperity heights follow a Gaussian distribution, (b) asperities are randomly distributed over the surface, and (c) contact deformation is purely plastic, with the harder surface assumed to indent the softer one. This model not only laid the foundation for subsequent theoretical developments but also captured, in a remarkably concise form, the essential parameters governing contact conductance:

$$h_c = 1.45\left(\frac{k_h m}{\sigma}\right)\left(\frac{P}{H}\right)^{0.985} \tag{5}$$

The right-hand side comprises two distinct components: the mechanical parameter P/H and the topographical parameter m/σ, whose product determines the thermal conductance. Here, P is the apparent pressure applied to the interface, and H is the hardness of the softer material. Larger P/H values correspond to greater real contact area, revealing the first fundamental trade-off in TIM design: the material must be sufficiently soft to deform under pressure in order to increase contact area, yet not so soft that it risks being extruded from the interface or undergoing pump-out failure during long-term operation. The parameter σ represents the root-mean-square roughness, characterizing the overall vertical variation of asperities, while m denotes the effective absolute mean slope of the surface, describing asperity steepness. Their ratio m/σ effectively captures the characteristic scale of surface topography—σ governs the gap thickness, and m determines the effective cross-sectional area of contact spots. Together, they provide a complete description of how readily heat flows across the interface. Notably, variations in the mean slope m imply different requirements for TIM deployment. On steep surfaces (high m), the valleys between asperities form deep, narrow V-shaped grooves. In such cases, the TIM must exhibit sufficient flowability and wettability to overcome capillary resistance under assembly pressure and fully infiltrate these geometrically confined regions, so as to prevent trapped air pockets. Conversely, on gentle surfaces (low m), macroscopic waviness and warpage become the dominant factors. The TIM thus relies more on its bulk compliance and sufficient bond-line thickness to bridge these large-scale topographic deviations, rather than on microscopic infiltration alone.

The model has several notable limitations. It treats the numerous asperities through statistical averaging, which implicitly assumes that contact spots are independent and non-interacting. In reality, the stress and heat flow fields of adjacent asperities become coupled when contact spot density is high. This simplification, therefore, introduces non-negligible errors. Moreover, parameters required by the model, such as the mean slope m, are difficult to measure accurately in practice, which to some extent limits its practical utility. In addition, the CMY model simplifies contact deformation by assuming purely plastic behavior. This assumption implies that the real contact area depends solely on the hardness of the softer material and is independent of the elastic modulus. However, for TIMs with polymer matrices, contact behavior often lies between elastic and plastic regimes. A purely plastic assumption fails to capture the evolution of the contact area accurately.

In 1974, Mikic systematically distinguished the effects of different deformation modes on thermal contact conductance [70]. Explicit expressions were derived for three cases: purely plastic deformation, plastic asperities on an elastic substrate, and purely elastic deformation. Criteria were also established to determine the prevailing deformation mode. The significance of this advance is its explicit statement that contact deformation is not a purely plastic process, but rather depends on the combined effects of load, material properties, and surface topography. In other words, designing TIMs requires attention to both hardness H and elastic modulus E: lower modulus materials achieve larger contact area through elastic deformation under the same load, yet this often comes at the cost of structural stability, such as long-term creep resistance [71]. However, Mikic's model treats deformation states as discrete categories. In reality, asperity contacts on engineering surfaces typically lie in a continuous transition zone between elasticity and plasticity: some asperities have plastically yielded while others remain elastic, with their proportions evolving continuously with load. Subsequent researchers introduced the plasticity index as a continuous parameter to describe the entire spectrum from purely elastic to purely plastic deformation [72].

For cured gel-type materials, the modulus is extremely low. Their deformation behavior exhibits both elastic and viscous characteristics [19,73]. To address this issue, Prasher et al. proposed an improved empirical formula for cured gel TIMs based on experimental investigations [71]. In this work, the shear modulus G is used in place of hardness H. Given that the thermal conductivity of the TIM is substantially lower than that of the metallic substrate, the harmonic mean thermal conductivity in the CMY model is approximated as $k \approx 2k_{\mathrm{TIM}}$,

leading to the following expression:

$$\frac{R_c k_{TIM}}{\sigma} = c\left(\frac{G}{P}\right)^n \quad (6)$$

where R_c is the total thermal contact resistance between the TIM and the two substrates, k_{TIM} is the thermal conductivity of the TIM, σ is the surface roughness of the substrate, and P is the applied pressure. The shear modulus G is derived from the storage modulus G' and loss modulus G'', i.e., $G = \sqrt{G'^2 + G''^2}$, while c and n are empirical fitting constants. This formulation directly correlates thermal contact resistance with the viscoelastic modulus of the material, revealing that lower modulus and higher pressure lead to lower contact resistance, thereby providing a theoretical basis for optimizing gel-type TIMs. Compared with the CMY model, this form is more suitable for describing the contact resistance behavior of low-modulus polymeric materials under pressure and lays the groundwork for subsequent discussions on modulus regulation and reliability design.

3.3. Multiscale filling

The statistical models discussed thus far (e.g., CMY) assume that surface topography can be fully described by a single characteristic length scale, such as the root-mean-square roughness (σ). In practice, engineering surfaces are multiscale, with roughness from the nanometer to the millimeter level [74,75]. Their contributions to thermal contact resistance differ fundamentally across scales. This insight has profound implications for thermal interface material design: an ideal material should effectively accommodate gaps at both scales.

The pioneering work of Clausing and Chao in 1964 provided the first systematic analysis of this issue. They distinguished between two distinct scales of surface imperfection on engineering surfaces: macroscopic waviness and microscopic roughness. When two surfaces are brought into contact, heat flow undergoes two constrictions: first, it is channeled into a limited number of macro-contact areas defined by the waviness, and then it is further constricted through numerous micro-asperity contacts within those areas. The total thermal resistance is the series sum of these two constriction resistances. Through systematic experiments, they found that the macroscopic resistance dominates, exceeding the microscopic resistance by a factor of 29 to 176 (ref. [76]). This leads to a clear design insight for thermal interface materials: a material must first and foremost be capable of filling the larger gaps. This demands adequate thickness and compliance to bridge the large-scale unevenness; otherwise, the dominant thermal resistance path will persist. In a later development, Majumdar and Tien proposed the M-T model [77]. Based on fractal geometry, this model uses a single parameter, the fractal dimension D, to quantitatively describe the statistical similarity of surface topography across length scales from nanometers to millimeters. It extends Clausing and Chao's "two-scale" dichotomy into a continuous spectral description and establishes a power-law relationship between thermal contact conductance and applied load.

4. Flexible and adaptive TIMs

The design of flexible TIMs initially addresses the coupled issue of bulk thermal conduction and interfacial contact. Polymer matrices typically exhibit good compliance and processability, allowing them to undergo compressive deformation under assembly pressure and conform to rough surfaces, which reduces contact thermal resistance. However, their inherently low thermal conductivity necessitates the incorporation of thermally conductive fillers, such as aluminum (Al), alumina (Al_2O_3), boron nitride (BN), graphene, carbon nanotubes (CNTs), or liquid metals, to create effective heat-flow pathways [15–17,23]. As the filler loading increases, the bulk thermal conductivity generally improves. Concurrently, the system may experience an increase in modulus, higher viscosity, challenges in reducing the BLT, filler aggregation, and elevated interfacial thermal resistance between the filler and matrix [12,15,18,19]. Consequently, the critical aspect of flexible TIM design is not merely to achieve high thermal conductivity or low modulus. Instead, it involves balancing the thermal network, matrix compliance, interfacial compaction, and long-term mechanical stability. This section is structured around this challenge. It begins by discussing matrix selection, filler organization, interfacial modification, high-loading rheology, and anti-fatigue networks in flexible polymer composite TIMs. It subsequently explores how self-adhesive and dynamically reconfigurable TIMs maintain effective contact under low pressure, zero pressure, or cyclic perturbations. In this context, flexible polymer composite TIMs establish a foundation for compliant and adaptive interface design.

4.1. Flexible polymer composite TIMs

The primary objective of flexible polymer-based TIMs is to create a deformable interface that facilitates effective heat conduction between the heat source and the heat sink. In the case of rough solid surfaces, the actual contact area is typically much smaller than the nominal contact area, which can lead to significant air entrapment and an increase in R_C. The advantage of a flexible matrix lies in its capacity to fill micron-scale gaps through mechanisms such as compression, segmental relaxation, and local flow, thereby ensuring that the heat flow paths established by filler networks are genuinely connected to the interface. Materials such as polydimethylsiloxane (PDMS) gels [16], brush-like PDMS composites [17], and three-branched polyurethane networks [19] exemplify this design principle. While an increase in filler loading often enhances thermal conductivity (k), it may concurrently elevate modulus, viscosity, and BLT, ultimately negating the advantages of improved bulk thermal conductivity [18,19]. Consequently, the design of flexible polymer-based TIMs should prioritize the interplay among three critical variables: matrix compliance, filler-based thermal pathways, and interfacial compaction. Although the term "fractal dimension" is used in both cases, it describes different physical objects. In the M–T model, the fractal dimension characterizes multiscale rough-surface topography and its influence on real contact area and contact conductance [77]. Here, the filler-network fractal dimension describes the internal spatial organization of fillers associated with thermal-path connectivity, stress transfer, and network flexibility. Within the present framework, these descriptions can be regarded as complementary but are not interchangeable.

The goal of designing flexible polymer-based TIMs is to minimize both bulk thermal resistance and interfacial contact resistance between the heat source and the heat sink. For rough solid–solid interfaces, the nominal contact area usually differs from the real contact area, and trapped air gaps strongly impede heat transfer [12]. Thus, the effective thermal resistance of a TIM must include both bulk and contact contributions, which implies that flexible polymer-based TIMs should not focus solely on increasing k; they must also reduce BLT under assembly pressure, fill micron-scale gaps, and maintain a stable real contact area [12,16–19].

In flexible polymer-based TIMs, the continuous phase is typically chosen from polymers with high segmental mobility and deformation adaptability. Examples such as PDMS gels [16], brush-like PDMS composites [17], short-dangling-chain-grafted elastomers [18], and three-branched polyurethane networks [19] demonstrate that low modulus, compressibility, and high stretchability enable materials to conform to rough interfaces under pressure and thereby reduce R_C. From the perspective of the Mikic model discussed in Section 3.2, a lower elastic modulus increases asperity deformation and the real contact area under the same pressure, shifting contact from the elastic regime toward elastic–plastic or plastic deformation [69,70]. For gel-like matrices, Prasher's viscoelastic extension further predicts that contact resistance decreases as shear modulus decreases and applied pressure increases

[71]. Therefore, chain lengthening, dangling-chain regulation, and low-crosslink-density design can be interpreted as mechanical routes for increasing real contact area rather than merely improving bulk flexibility.

The flexible matrix does more than carry fillers; it provides the mechanical basis for converting bulk thermal pathways into low-R_C interfacial contacts [16–19]. Matrix design first determines whether a material can rapidly conform to a rough interface under assembly load. Extending polymer chain segments [16] increases the effective chain length between crosslinking points, lowers modulus, and improves tensile deformability. Dangling-chain regulation [18,78] promotes segmental relaxation and interfacial sliding while increasing energy dissipation under cyclic loading. Three-branched polyurethane networks [19] preserve compliance and stretchability after fillers are incorporated. Bottlebrush-like polysiloxanes [15] reduce the flow resistance of highly filled composites via a loose backbone and long side chains, allowing the system to retain thixotropic behavior even at high Al_2O_3 loadings. Hyperbranched multilevel networks suppress filler aggregation and lower interfacial thermal resistance by enhancing interactions between the elastomer and fillers [29]. All of these strategies aim to minimize the deformation penalty introduced by fillers and to maintain effective contact under load.

To raise bulk k, flexible polymer TIMs must incorporate thermally conductive fillers. Different fillers address distinct design goals. Spherical Al fillers promote low-resistance thermal networks in elastomers such as PDMS while preserving processability and mechanical energy dissipation [16,78]. Al_2O_3 fillers are inexpensive, electrically insulating, and compatible with high loadings, but high filler content increases viscosity and BLT unless polymer architecture, filler networks, or surface-energy matching are implemented [12,63]. Boron nitride nanosheets (BNNS) or BN fillers suit electrically insulating flexible TIMs, but interfacial thermal resistance between nanosheets and between nanosheets and the polymer matrix must be controlled [20,79–81]. Reports of BN/graphite layered structures [82], densely packed flexible films [83], and dual-field-aligned graphene fibers [23] show that low modulus does not necessarily imply low thermal conductivity. When high-k fillers are organized into through-plane pathways and either the fillers or the matrix retains low stiffness, materials can achieve high-κ alongside low R_C.

The spatial organization of fillers determines whether heat can be transported through the polymer matrix along continuous thermal pathways. In flexible polymer-based TIMs, randomly dispersed fillers often fail to form efficient through-plane heat paths, particularly at low filler loadings, where limited contact between fillers restricts further improvement in k. Thus, orientation, dense packing, and multiscale assembly are primary strategies for improving through-plane heat transfer. Vertically aligned BN/graphite layered silicone rubber [82] preserves BN and graphite film alignment through stacking and cutting, yielding high through-plane thermal conductivity and a low compressive modulus. Densely packed flexible films [83] enhance through-plane transfer by tightly organizing Al_2O_3 and two-dimensional fillers while maintaining a low Young's modulus. Dual-field-aligned graphene fibers (GFs) [23] exploit the high intrinsic k and low stiffness of GFs to achieve high through-plane k, low compressive modulus, and reduced contact thermal resistance at low filler loadings. These studies indicate that fillers in flexible polymer-based TIMs should not act merely as high- k additives; they must be arranged into conductive structures that span the through-plane direction without substantially compromising compliance [23,82,83].

After fillers form conductive pathways, heat must still cross many filler-matrix and filler-filler interfaces. Poor dispersion, mismatched surface energies, or weak interfacial bonding can cause local aggregation that breaks continuous thermal pathways. Interfacial phonon scattering raises microscopic thermal resistance, and highly filled systems often exhibit increased viscosity, yield stress, and BLT [12,20,79]. Thus, modifying the filler-matrix interface is a key strategy to lower composite thermal resistance. Surface-functionalized BNNS [20] (Fig. 3a(i)) reduce interfacial thermal resistance at BNNS junctions and at BNNS-matrix interfaces while preserving BNNS's high intrinsic thermal conductivity (Fig. 3a(i, ii)), yielding thermal conductivities of about 21–25 W m^{-1} K^{-1} and a low Young's modulus. Perfluoropolyether (PFPE)-modified BNNS [79] enhance BNNS dispersion in silicone rubber, reduce nanosheet-matrix interfacial thermal resistance, and improve thermal conductivity. Furthermore, self-assembled monolayer-modified aluminum oxide (SAM-modified Al_2O_3) [12] (Fig. 3b) provides a quantifiable molecular design rule by tuning surface-energy matching. C4-SAM better matches the surface energy of the silicone-oil matrix, suppresses Al_2O_3 agglomeration, lowers yield stress, and enhances shear thinning. At the same pressure, the BLT decreases from about 608 μm in the unmodified system to about 20 μm, and the resulting R_{EFF} reaches 0.142 cm^2 K W^{-1}. These findings show that filler surface layers not only reduce microscopic interfacial thermal resistance but also alter macroscopic effective thermal resistance via changes in dispersion, rheology, and BLT [12,20,79].

Interfacial modification can reduce filler–matrix mismatch, but increasing filler loading introduces new rheological challenges. High loading promotes filler contacts and raises k, yet it also raises viscosity, impedes shear spreading, hinders BLT reduction, and weakens thixotropic recovery [15,22,31,65]. Thus, in highly filled TIMs, k enhancement must be co-designed with compressibility and thixotropic behavior. In core-shell hybrid fillers, deformable liquid metal localized at the polyurethane–polydimethylsiloxane/aluminum oxide composites (PUPDM/Al_2O_3 composites) interface enhances segmental mobility and shortens the relaxation time, in highly filled systems, and preserves thermal conduction and electrical insulation at high Al_2O_3 loading [22] (Fig. 3c). Ce/Ti-modified MgO (CT-MgO) fillers improve mixing efficiency with PDMS, enabling an 80 vol% filled system to reach 8.2 W m^{-1} K^{-1} while retaining a thixotropic state [31] (Fig. 3d). Bottlebrush-like polysiloxane/Al_2O_3 systems extend this strategy toward the high-loading limit [15]. Their low-viscosity polymethylvinylsiloxane grafted with octadecanethiol side chains (PMVS-ODT) supports an Al_2O_3 loading of up to 87.8 vol%; at 79.4 vol%, the material still shows good compliance and thixotropy, achieving a thermal conductivity of 8.181 W m^{-1} K^{-1} and an R_C of 20.9 mm^2 K W^{-1} under 20 psi. These results show that the key bottleneck in highly filled systems is not whether there are enough fillers, but whether the material can spread rapidly under shear and assembly pressure, reduce the BLT, and recover shape stability after standing [15,22,31,65].

Simply lowering matrix viscosity or altering a single filler surface is therefore insufficient. Highly filled systems must alternate between static stability and shear-induced flow. During assembly they must spread and fill gaps like a liquid; during service they must preserve shape and maintain the thermal network like a solid. Hierarchical filler rheological design provides an alternative route for highly filled flexible TIMs. Multimodal aluminum nitride (AlN)/PDMS yield-stress composite fluids [64] (Fig. 3e) employ large, medium, and small AlN particles for hierarchical packing, so that small particles occupy voids between larger ones, increase filler–filler contact density, and form a dynamic thermal network. The quaternary AlN/PDMS system attains a thermal conductivity of 12.0 W m^{-1} K^{-1} at 84.7 vol% while exhibiting low viscosity, tunable yield stress, and robust thixotropic recovery (Fig. 3e(i)). Under shear the network disassembles and flows like a liquid, which facilitates dispensing and gap filling; after standing the network reconstructs and regains solid-like stability (Fig. 3e(ii)). These findings imply that designing highly filled TIMs requires evaluating not only maximum filler loading but also shear thinning, yield stress, recovery after standing, and BLT. The CMY framework also clarifies why rheological optimization is inseparable from filler packing. Although high filler loading improves bulk thermal conductivity, the associated increases in effective hardness, yield stress, and BLT reduce the pressure-to-hardness ratio and limit asperity deformation [69]. Meanwhile, insufficient flow leaves the macroscopic waviness and microscopic roughness identified by Clausing

and Chao only partially filled [76]. Shear thinning and thixotropic recovery therefore lower contact resistance by enabling pressure-driven spreading during assembly while preserving network stability after the interface has been formed.

The strategies discussed above primarily address initial assembly and short-term heat transfer. In real applications, TIMs also experience thermal cycling, compression cycling, vibration, and repeated deformation. If the filler network is too sparse, thermal pathways cannot be sustained; if it is too dense, the material becomes rigid and brittle and may crack under cyclic loading [63]. Thus, flexible polymer-based TIMs must preserve the mechanical stability of both the thermal network and the interfacial contact. A fractal filler-network design tailors filler size and spatial distribution in Al_2O_3/PDMS (Fig. 3f(i)) to control the network's fractal dimension (Fig. 3f(ii)), balancing filler contact, stress transfer, and network flexibility at high loading. At 96 wt% Al_2O_3, an Al_2O_3/PDMS system with a moderate fractal dimension attains a low Young's modulus of about 131.4 kPa, a fracture energy of 121.71 J m^{-2}, a fatigue threshold of 72.83 J m^{-2}, and a thermal conductivity of about 7.0 W m^{-1} K^{-1}. These results indicate that an appropriate network hierarchy can simultaneously organize thermal pathways and dissipate stress, enabling highly filled systems to retain thermal conductivity without excessive rigidification.

Fractal networks emphasize the spatial connectivity of fillers, but achieving fatigue-resistant contacts also requires design at the level of polymer segments and filler–interface sliding. Short-dangling-chain/Al filler synergistic networks [78] address this need by influencing crack propagation. Short dangling chains [78] increase the effective chain length between crosslink points, while Al fillers [78] pin cracks and establish a thermally conductive network. Combined, these features raise fracture energy and fatigue threshold and increase energy dissipation via crack pinning and interfacial slippage. PDMS/Al composites can reach a Young's modulus of about 0.16 MPa, a fracture energy of 3316 J m^{-2}, a fatigue threshold of 1052.56 J m^{-2}, and a thermal resistance near 0.12 cm^2 K W^{-1}. For flexible polymer-based TIMs, anti-fatigue design ensures that low R_C persists not only under the initial assembly pressure but also after thermal cycling, vibration, and repeated deformation.

In summary, the design of flexible polymer-based TIMs can be framed at four levels. Flexible matrices provide the mechanical foundation for low R_C by enabling segmental relaxation and morphological adaptation [16–19]. Thermally conductive fillers create bulk heat-flow pathways via orientation, dense packing, and the use of low-stiffness, high-k components [15,20,23,82,83]. Filler surface modification lowers effective thermal resistance by coordinating dispersion, interfacial thermal resistance, rheology, and BLT [12,20,79]. Highly filled networks and anti-fatigue architectures further secure low BLT, low R_C, and long-term stability [15,63,64,78]. If interfacial contact additionally depends on self-adhesion, dynamic bonds, or reversible interfacial reconstruction, the focus moves from flexible polymer matrix design to self-adhesive and dynamically reconfigurable TIMs.

4.2. Self-adhesive and dynamically reconfigurable TIMs

In low-preload, zero-pressure assemblies and flexible electronic interfaces, TIMs cannot rely on external loads to sustain long-term contact. Silicone-based TIMs are widespread, but weak interfacial bonding, oil bleeding, thermal aging, thermally induced micropore growth, and debonding undermine interfacial stability [84]. For soft, planar electronic devices, materials must also combine self-adhesion, elasticity, stretchability, and low interfacial thermal resistance. Insufficient adhesion and elasticity limit synchronous deformation between the heat-spreading layer and the soft device, which raises interfacial thermal resistance [34]. Moreover, the coupled constraint between interfacial heat transfer and mechanical transfer makes it difficult for polymer TIMs to achieve high thermal conductivity, self-adhesion, and stretchability simultaneously [85]. Thus, the design of self-adhesive, dynamically reconfigurable TIMs does not aim solely to increase adhesion strength; it seeks to enable active real contact under low pressure and to maintain low R_C after temperature, stress, or interfacial morphology changes [34,35,84–86]. Recent studies have developed intrinsic adhesive matrices, viscoelastic heat-spreading layers, bioinspired adhesive interfaces, and dynamic-bond reconfigurable networks to convert interfacial adhesion into stable, low-impedance heat-transfer pathways [34,35,84–86]. Classical CMY and Mikic models describe load-controlled contact and therefore do not explicitly include adhesion [69,70]. Nevertheless, self-adhesive TIMs can be interpreted as generating an interfacial normal traction that supplements or partly replaces externally applied pressure. This traction brings more asperities into contact and maintains the real contact area after unloading, while viscoelastic relaxation allows the interface to continue conforming with time. Accordingly, adhesion strength should be considered together with modulus, relaxation behavior, and surface topography, rather than treated as an independent performance metric.

Intrinsic adhesive matrices provide a direct route to low-pressure contact. Poly(ionic liquid) (PIL) systems use ionic interactions, strong interfacial adhesion, and thermal stability to alleviate the insufficient bonding of silicone-based TIMs on metal or semiconductor surfaces [84,86]. The P[Im_{12}V]TFSI matrix (Fig. 4a) constructed by Lin et al. showed adhesion strengths of 5.52 and 3.92 MPa to copper (Cu) and silicon (Si), respectively. After silver (Ag) fillers were introduced, the P[Im_{12}V] TFSI/Ag composite still retained adhesion strengths of 1.19 and 1.26 MPa on Si and Cu at 80 vol% filler loading, while achieving a thermal conductivity of 17.2 W m^{-1} K^{-1}. Another poly(1-butyl-3-vinylimidazolium) bis(trifluoromethylsulfonyl)imide (P[Im_4V]NTf_2) system reached adhesion strengths of 7.7 and 8.3 MPa to Cu and Si, respectively. Its Al-filled composite exhibited a thermal conductivity above 3 W m^{-1} K^{-1} and maintained an adhesion strength of about 0.6 MPa on Cu, steel, and glass, clearly higher than the approximately 0.05 MPa of silicone-based TIMs [86]. These studies indicate that PIL matrices can combine interfacial adhesion, filler compatibility, thermal stability, and reversible ionic interactions, providing a material basis for self-adhesive TIMs beyond silicone-based systems.

Strong adhesion must still be coupled with deformation adaptability and thermal pathways. For flexible and planar electronics, an interfacial layer lacking viscoelasticity and stretchability can undergo local debonding and contact-area decay during thermal cycling or device deformation [34]. Wang et al. developed a thermochromic nacre-like viscoelastic nanocomposite film in which a layered thermally conductive network is embedded in a soft viscoelastic matrix (Fig. 4b) [34]. The soft matrix enables self-adhesion, stretchability, and self-healing, whereas the layered network preserves efficient in-plane heat spreading. The obtained soft thermochromic composite (STC) film shows an in-plane thermal conductivity of about 30 W m^{-1} K^{-1}, a low thermal contact resistance of about 12 mm^2 K W^{-1}, and can reduce the temperature of soft electronic devices by about 20 °C compared with a polyimide substrate [34]. This result indicates that a self-adhesive heat-spreading layer must simultaneously provide interfacial fixation, deformation following, and heat spreading. A single adhesion-strength value cannot fully describe its thermal-management capability.

Segmental-structure design integrates adhesion, elasticity, and thermal conduction within a single polymer network. Polyphenol-rich flexible elastomer/aluminum oxide composites (PRFE/Al_2O_3 composites) [85] exploit the synergy between flexible PDMS segments and rigid polyphenol units to establish efficient thermal pathways at high filler loadings while preserving low modulus, strong adhesion, and toughness. Their thermal conductivity is 5.4 W m^{-1} K^{-1}, and their thermal resistance is about 0.29 cm^2 K W^{-1}. In contrast to PIL systems, these polymer frameworks prioritize concurrent control of interfacial mechanical transfer and heat-flow transfer through chain-segment engineering. Flexible segments enable morphological adaptation, rigid adhesive units strengthen interfacial bonding, and the filler network maintains the bulk heat-flow pathway. This approach offers an alternative molecular design

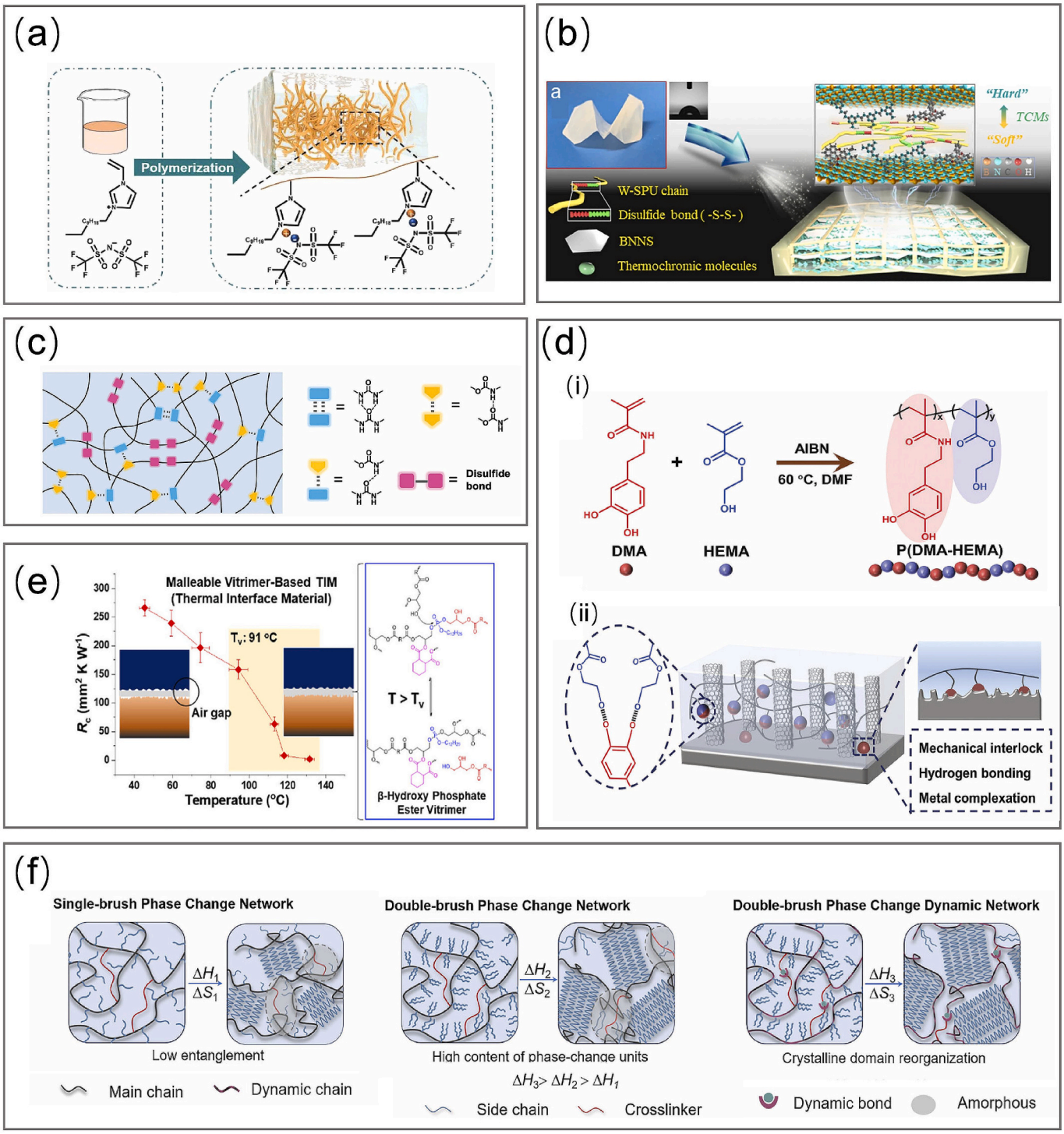

Fig. 4. Representative molecular and network designs for self-adhesive and dynamically reconfigurable flexible thermal interface materials. (a) Molecular structures of the ionic liquid monomers and the resulting P[Im_{12}V]TFSI polymer network, highlighting its stretchability, interfacial adhesion, and self-healing capability [84]. (b) Design of the thermochromic and viscoelastic nacre-like STC membrane, in which thermochromic molecules mediate the interactions between the soft W-SPU matrix and rigid BNNS layers [34]. (c) Dynamic PUUI network stabilized by multiple hydrogen-bonding interactions and reversible disulfide bonds [35]. (d) Bio-inspired P(DMA-HEMA)/VACNT adhesive composite: (i) synthesis of the P(DMA-HEMA) copolymer and (ii) its strong substrate adhesion enabled by hydrogen bonding, metal coordination, and mechanical interlocking [36]. (e) Temperature-dependent reduction in the thermal resistance of a β-hydroxy phosphate ester vitrimer-based TIM [88]. (f) Topological evolution from single-brush networks to double-brush and double-brush dynamic phase-change polymer networks [26].

concept for highly filled, self-adhesive TIMs.

Introducing dynamic bonds into a self-adhesive system enhances the interface's responsiveness to temperature and mechanical stress. Wu et al. developed a poly(urethane-urea-imide) (PUUI) adhesive TIM that combines a dynamic hydrogen-bond network with reversible disulfide bonds (Fig. 4c) [35]. Upon heating, these dynamic interactions promote chain rearrangement and allow the TIM to form adaptive contact with metal surfaces. The material attains a maximum adhesion strength of 7.39 MPa on aluminum. When filled with AlN and liquid metal, it achieves a thermal conductivity of 3.87 W m^{-1} K^{-1} and a zero-pressure

thermal contact resistance of 22.1 mm^2 K W^{-1}. The interface evolves from its initial adhesive state to a more complete, conformal contact upon heating.

The adhesive layer must also form an effective connection with the internal high-conductivity network. If the adhesive matrix improves bonding only at the external surface and fails to bridge the oriented thermal pathways, enhanced interfacial adhesion will not reduce the effective thermal resistance [36]. Zhang et al. combined a bioinspired adhesive polymer with VACNT-oriented heat-flow channels. They synthesized a poly(dopamine methacrylate-*co*-hydroxyethyl methacrylate) copolymer [P(DMA-HEMA)] inspired by snail and mussel adhesion and incorporated it into vertically aligned carbon nanotubes (VACNTs) to form P(DMA-HEMA)/VACNT composites (Fig. 4d). In this system, P(DMA-HEMA) supplies surface adhesion via hydrogen bonding and mechanical interlocking, while catechol groups strengthen interfacial bonding with VACNTs through π-π interactions. The composite reaches a through-plane thermal conductivity of 21.46 W m^{-1} K^{-1} and a thermal contact resistance of 20.27 mm^2 K W^{-1} under zero pressure [36]. These results indicate that self-adhesive designs for low-pressure interfaces must connect the external solid surface and the internal oriented thermal pathways so that interfacial adhesion, filler contact, and through-plane heat transfer operate in concert.

Molecular adhesive units can also improve local conformity at rough interfaces and at filler–matrix boundaries. Regulating dangling-chain length [87] enhances chain-segment adaptation to microscopic filler and substrate roughness, reduces phonon scattering, and yields a contact thermal resistance of 0.48 ± 0.08 cm^2 K W^{-1} and a thermal conductivity of 4.57 ± 0.03 W m^{-1} K^{-1}. Gecko-inspired comb-like copolymers with short dangling ends [30] act at both the TIM/substrate and polymer/filler interfaces. They increase thermal boundary conductance and dissipate vibrational energy via van der Waals bond dissociation and a broadened relaxation spectrum. Grafted amorphous alkyl chains [32] (Fig. 4d) enhance cross-interface heat transfer by improving interfacial adsorption and surface-energy matching. These studies shift the focus from macroscopic peeling strength to interactions between chain segments and surfaces, thereby enabling molecular design to regulate real contact area, interfacial scattering, and vibrational dissipation [30,32,87].

Self-adhesion ensures initial interfacial contact, but thermal cycling, mechanical disturbance, and changes in surface roughness continue to modify the contact state. Dynamic covalent networks enable segmental rearrangement and interfacial recontact at service temperatures, thereby reducing R_C [26,35,88]. Cha et al. reported a β-hydroxy phosphate ester vitrimer in which associative dynamic covalent bond exchange occurs above the topology freezing transition temperature (Fig. 4e) [88]. This dynamic exchange imparts plasticity and conformability to the thermoset matrix. As the temperature rises from 45 °C to 132 °C, the total thermal resistance of this system falls from 516 mm^2 K W^{-1} to 8.45 mm^2 K W^{-1}, a reduction of nearly two orders of magnitude. This change primarily reflects improved interfacial conformability and a pronounced decrease in R_C. The result demonstrates that dynamic covalent bond exchange can convert operating temperature into a driving force for interfacial reconstruction, allowing thermoset TIMs to achieve low contact thermal resistance while maintaining structural integrity.

Fast-relaxing dynamic networks further enhance the efficiency of thermally triggered interfacial reconstruction. Liu et al. designed a double-brush phase-change polymer network with two types of dynamic bonds, including B-O-B and Si-O-B linkages [26]. The resulting double-brush phase-change polymer (PVBS-TMC) network reaches an ultrafast relaxation time of 0.8 s at 80 °C and exhibits a high phase-change enthalpy of 240.7 J g^{-1}. When this dynamic polymer is combined with graphene foam films, the composite lowers interfacial thermal resistance via phase-change–induced modulus reduction, a low-entanglement dynamic matrix, and adaptive filling ability (Fig. 4f). It also demonstrates superior thermal-management efficiency compared with commercial materials [26].

In addition to covalent dynamic networks, dynamic coordination and supramolecular interactions can also form reconfigurable interfaces. Ji et al. introduced carboxyl/aluminum and carboxyl/zinc oxide coordination bonds into a PDMS elastomer [89]. Strong interfacial interactions decrease polymer–filler interfacial thermal resistance, while the dissociation and reformation of dynamic coordination bonds restore toughness and compliance lost to high filler loading. The system attains a thermal conductivity of 2.37 W m^{-1} K^{-1}, a toughness of 1073 J m^{-2}, a stress of 0.11 MPa, an elongation at break of 910%, and reprocessability [89]. Lignin-induced supramolecular self-assembled systems enhance viscoelasticity and interfacial adaptability through dynamic supramolecular interactions, reducing contact thermal resistance by 71.9%, increasing thermal conductivity by 18.8% relative to VTCP, and lowering CPU temperature by about 13.1 °C compared with a high-performance commercial TIM [33]. Together, these results indicate that dynamic interactions can concurrently influence interfacial thermal resistance, mechanical dissipation, and long-term adaptability, but they must be integrated with effective thermal pathways in the design.

To address insufficient initial contact, thermal-cycle-induced debonding, and contact-state decay at low-pressure interfaces, researchers have pursued several strategies centered on self-adhesive matrices, bioinspired adhesive interfaces, dynamic bond exchange, and thermally triggered reconfiguration. PIL matrices [84,86] deliver strong adhesion and serve as alternatives to silicone-based systems. Viscoelastic nacre-like films [34] and PRFE segmental structures [85] combine adhesion, elasticity, and heat spreading. PUUI dynamic adhesive networks [35], P(DMA-HEMA)/VACNT composites [36], and dangling-chain/comb-chain designs [30,87] link adhesive interfaces to real contact area and internal thermal pathways. β-Hydroxy phosphate ester vitrimers [88], double-dynamic-bond double-brush networks [26], and open-encapsulated G/APM/PEG [90] demonstrate that thermally triggered chain rearrangement, rapid relaxation, and exposed wetting can transform dynamic reconstruction into reduced R_C. Overall performance of self-adhesive and dynamically reconfigurable TIMs depends on the interplay among adhesion strength, relaxation time, interfacial wetting, mechanical retention, and thermal networks. If interfacial adaptation additionally involves large-scale softening, flow-based gap filling, or liquid bridging of the matrix, the low-resistance mechanism falls within the domain of gap-filling TIMs.

5. Gap-filling strategies of TIMs

Even after flexible matrices and improved interfacial adhesion establish initial contact, residual voids, assembly tolerances, and BLT at rough interfaces can still limit a TIM's effective thermal performance. A solid TIM with high bulk thermal conductivity may still leave air gaps if the interface is not fully filled, causing local heat-flow constriction and additional temperature drops along the heat source-TIM-heat sink pathway [28,91]. Thus, the primary role of gap-filling TIMs is to displace air and restore continuous contact by softening, flowing, wetting, or forming liquid bridges. Different gap-filling media offer distinct benefits and drawbacks. Phase-change materials (PCMs) and thermally softened materials lower modulus and improve interfacial compliance within the operating temperature range [42,92,93]. Greases, gels, and pastes use controlled rheology to form low-BLT contact layers under assembly pressure [94]. Liquid metals further reduce contact thermal resistance via flow, wetting, and thermal-bridge formation, but they introduce risks of leakage, electrical shorting, and encapsulation-stability challenges [9]. Accordingly, this section first examines phase-change and thermally softened TIMs, then addresses the rheology-BLT coupling of pastes and gels, and finally discusses the wetting, bridging, and confined-stability strategies for liquid-metal-based TIMs.

5.1. Phase-change and thermally softened TIMs

In gap-filling TIMs, phase changes and thermal softening primarily

convert operating or packaging temperature into interfacial compliance. When a material undergoes a solid–liquid transition, a glass transition, or surface softening within a given temperature window, its modulus falls and its wettability improves. As a result, microscopic voids at rough interfaces are more readily filled, yielding a lower R_C [92,93,95,96]. Huang et al. showed that, under 70 °C, 50 N, and a contact area of 400 mm^2, the modulus drop caused by the solid–liquid transition of stearic acid reduced the contact thermal resistance to 2.39×10^{-4} K m^2 W^{-1} by improving interfacial conformity [92]. Ou et al. reported that a silicone wax phase transition produced a 99.09% change in modulus and a corresponding 66.91% reduction in contact thermal resistance [93]. These findings indicate that the primary value of temperature-responsive materials lies in reconstructing the contact state, not solely in altering the bulk thermal conductivity [92,93]. The theoretical basis of thermal softening can be understood by combining the deformation framework with the multiscale filling concept in Section 3.3. A temperature-induced decrease in modulus increases asperity deformation under the same load, thereby enlarging the real contact area. Simultaneously, the softened phase can infiltrate microscopic valleys and accommodate macroscopic waviness that cannot be represented by a single roughness parameter. Thus, phase transition lowers contact resistance through both contact-mechanics regulation and multiscale gap filling, rather than through a change in bulk thermal conductivity alone.

Thermally softened interface materials further clarify the causal link among modulus reduction, interfacial conformity, and R_C reduction. The poly(ethylene-*co*-vinyl acetate)/epoxy/poly(ethylene-co-vinyl acetate) (PEVA-EP-PEVA) thermally softened TIM developed by Kim et al. [96] employs temperature-triggered surface softening to progressively conform to rough interfaces during heating (Fig. 5a). As the surface modulus falls from 26.28 GPa to 2.10 GPa, R_C decreases from 108.41 to 78.73 mm^2 K W^{-1}. At 100 °C, the surface modulus further drops to 0.19 GPa and R_C falls to 0.17 mm^2 K W^{-1}, while k_{TIM} declines only from 106.5 to 82.8 W m^{-1} K^{-1}; the total heat flux increases by 2030%. This observation is particularly important for phase-change or softening TIMs, since a modest reduction in bulk k can be compensated by a large

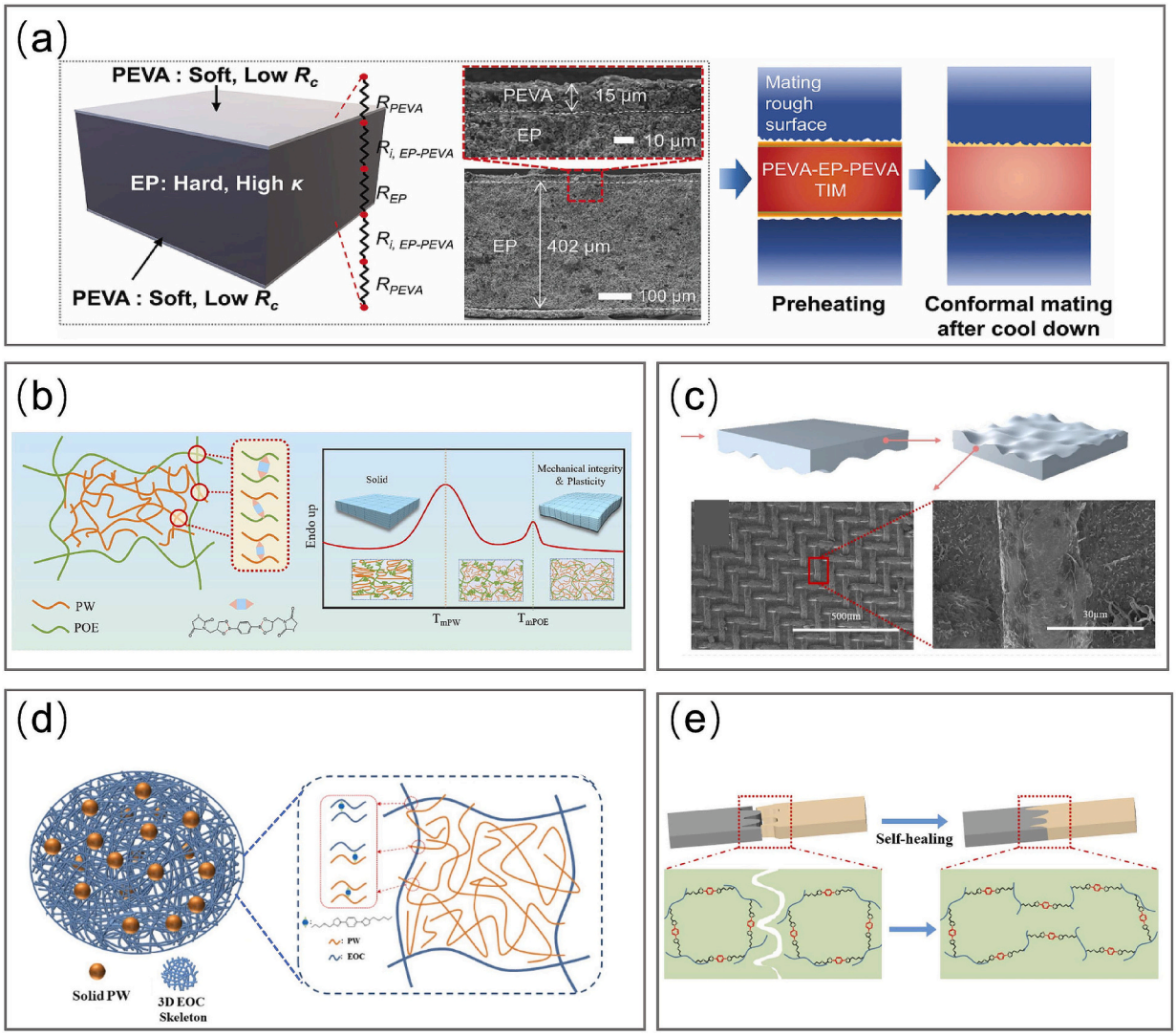

Fig. 5. Thermally activated interfacial adaptation through surface softening, phase-change plasticity, and dynamic network reconfiguration. (a) High-temperature-softening PEVA–EP–PEVA TIM, showing its soft-skin/hard-core architecture, cross-sectional morphology, thermal-resistance network, and thermally induced conformal contact with a rough surface [96]. (b) Vitrimeric PW/POE PCM, illustrating the dynamic network structure and thermally enabled mechanical integrity and plasticity arising from phase transition and boronic-ester exchange [27]. (c) Thermally induced surface patterning of the hybrid-filled vitrimeric PW/POE composite, with SEM images of the microstructured PVDF template and the inversely replicated composite surface [27]. (d) Structural design of the PW/ethylene–octene copolymer (EOC) thermal interface phase-change material, in which PW domains are confined within a boron-ester-crosslinked three-dimensional EOC skeleton [99]. (e) Self-healing mechanism enabled by thermally activated boron-ester bond exchange and dynamic network rearrangement [99].

decrease in interfacial thermal resistance, leaving the effective thermal resistance dominated by improved interfacial contact.

Temperature-triggered softening can also introduce risks to shape stability and cause leakage. If a phase-change material flows freely after softening, it may fill gaps briefly but can also lead to material loss, pump-out, thickness changes, and eventual failure after repeated assembly [27,92,97–100]. Thus, effective phase-change TIMs typically confine softening within crosslinked networks, supporting frameworks, or flow-restricting structures so the material lowers R_C while preserving mechanical integrity and repeatable adaptability [27,92,97,99].

Vitrimeric PCMs offer a direct solution to this challenge. Peng et al. developed a vitrimeric paraffin wax/polyolefin elastomer (PW/POE) system that combines the solid–liquid phase change of PW with dynamic covalent bond exchange in the POE network [27]. The PW phase transition reduces the composite modulus, while POE melting triggers dynamic bond exchange (Fig. 5b). At 80 °C and 13 kPa the material undergoes plastic deformation under low stress, conforms to rough heat-source and heat-sink surfaces, and forms an interlocked interface that lowers thermal contact resistance (Fig. 5c). Crucially, the softening does not produce unconstrained flow but instead yields reconfigurable deformation governed by the dynamic network. As a result, the material acquires interfacial adaptability during packaging while preserving a three-dimensional supporting framework that prevents structural collapse after the phase transition.

Borate-ester dynamic crosslinking combines shape stability, self-healing, and interfacial adaptation. Huang et al. designed a thermal interface phase change material that incorporates a borate-ester crosslinked framework into a PW/EOC system [99] (Fig. 5d), allowing the phase-change material to retain mechanical integrity and suppress leakage above the EOC melting temperature. The PW phase transition reduces the modulus, and borate-ester bond exchange, activated by heat, enables self-healing and shape memory (Fig. 5e); consequently, the material can flow into rough interfaces under small stress and form interlocked contacts. In device tests, this TIPCM cooled a simulated CPU to 67 °C at 5 V. Compared with vitrimeric PW/POE PCMs, TIPCM highlights the role of a dynamic crosslinked network in leakage control, thermal repair, and repeatable interfacial adaptation. Together, the two studies indicate that phase-change softening must be engineered alongside network reconstruction and shape retention.

Latent-heat buffering can further mitigate transient thermal shock, but its engineering effectiveness requires low R_C and efficient thermal pathways. If a material offers high phase-change enthalpy yet lacks sufficient interfacial contact, heat cannot quickly enter the phase-change matrix and latent-heat absorption cannot translate into device-level cooling [26,92,101,102]. Vertically aligned CFs/PEG systems address this by using magnetic-field-induced through-plane alignment of carbon fibers to enhance the through-plane thermal conductivity of the PEG phase-change matrix [101]. They also exploit the self-adaptive behavior of PEG upon heating to lower the thermal resistance to 1.12 $cm^2\ K\ W^{-1}$ while maintaining a melting enthalpy of 118.03 $J\ g^{-1}$. Hierarchically encapsulated phase-change films [102] combine high enthalpy with ultra-flexibility in the working state via an encapsulated architecture, which stabilizes the phase-change filling process. Double-brush phase-change polymer networks [26] employ B-O-B and Si-O-B dynamic bonds to attain an ultrafast relaxation time of 0.8 s at 80 °C and a high phase-change enthalpy of 240.7 $J\ g^{-1}$. When integrated with graphene foam films, PVBS-TMC/GF lowers interfacial thermal resistance through phase-change-induced modulus reduction, a low-entanglement dynamic matrix, and adaptive filling capability [26]. Together, these studies indicate that latent heat, rapid relaxation, and effective interfacial filling must operate in concert to translate the intrinsic heat-storage capacity of phase-change materials into practical heat dissipation [26,101,102].

Phase-change materials must preserve continuous heat-transfer pathways in their softened state. Phase transitions alter matrix volume, chain-segment mobility, and filler positions, and randomly dispersed fillers can locally rearrange during repeated melting and solidification, degrading the thermal network [24,44,97,103]. To prevent this, researchers employ three-dimensional supporting networks, oriented fillers, or continuous frameworks that maintain thermal pathways after phase transition. For example, a three-dimensional BN network in vitrimeric PCMs preserves continuous thermal channels after PW undergoes the solid–liquid transition, enabling reliable heat transport while retaining phase-change adaptability [97]. Solid–solid phase-change conductive films improve shape stability by avoiding large-scale liquid flow [103]. Vertically aligned graphene/paraffin layered composites provide vertical carbon pathways that align the phase-change matrix with the interfacial heat-flow direction [44]. Three-dimensional vertical carbon networks further show that ordered thermal frameworks support through-plane heat transfer and reduce contact thermal resistance in the softened or phase-change state [24]. These strategies constrain temperature-triggered compliance into repeatable, thermally conductive architectures, preventing the softened state from producing only flow without sustained heat dissipation.

In summary, to mitigate air gaps at rough interfaces, transient thermal shock, and poor contact under low preload, researchers have developed approaches including phase-change softening [92,93], thermally softened surface layers [96], vitrimeric reconfigurable encapsulation [27], borate-ester-crosslinked self-healing TIPCM [99], high-enthalpy fast-relaxing phase-change networks [26], and shape-stable thermal frameworks [24,44,97,103]. These strategies aim to lower modulus, improve wetting, and fill rough interfaces within the operating temperature window, while preserving shape stability and continuous heat transfer via crosslinked networks, supporting frameworks, or constrained flow. The performance of phase-change and thermally softened TIMs ultimately hinges on simultaneous fulfillment of three criteria: temperature-triggered interfacial compliance, anti-leakage and repeatable adaptation in the softened state, and low-resistance thermal pathways throughout the softened matrix.

5.2. Greases, gel, and paste-type TIMs

Greases, silicone greases, pastes, and gel-type TIMs reduce interfacial thermal resistance by flowing, spreading, or deforming locally under assembly pressure [104,105]. These materials penetrate microscopic surface voids, replace the air trapped between rough mating surfaces with a continuous heat-transfer medium, and form a thinner BLT [58]. Because real solid surfaces contact only locally, air-filled gaps strongly hinder heat transfer; flowable TIMs improve interfacial transport by filling these gaps and reducing the thickness of the interfacial layer. This function is also strongly affected by interfacial roughness. For relatively smooth surfaces, compressibility, spreading ability, and the ability to form a small BLT are more important; for rougher surfaces, the material must additionally fill deeper valleys and maintain effective heat conduction through a thicker paste layer. The performance of these TIMs is therefore governed by the combined effects of surface roughness, filler morphology, spreading ability, compressibility, and BLT, rather than by filler thermal conductivity alone. Silicone greases can fill interfacial gaps on the order of 100 μm, while flexible gel TIMs can more fully conform to contacting surfaces. Their main advantage therefore lies in interface formation as well as bulk heat conduction. For greases, gels, and pastes, Prasher's viscoelastic formulation provides a more appropriate interpretation than a purely plastic CMY description, because their contact response depends on shear modulus, pressure, and time-dependent flow [71]. The two-scale analysis of Clausing and Chao further indicates that these materials must first bridge macroscopic waviness and then penetrate microscopic roughness [76]. Consequently, viscosity, yield stress, and BLT determine whether the material reaches both length scales; excessive resistance to flow can preserve large unfilled regions even when the bulk thermal conductivity is high.

Gel-type TIMs retain gap-filling ability while providing better shape retention than conventional greases. Cai et al. developed a PDMS/Al

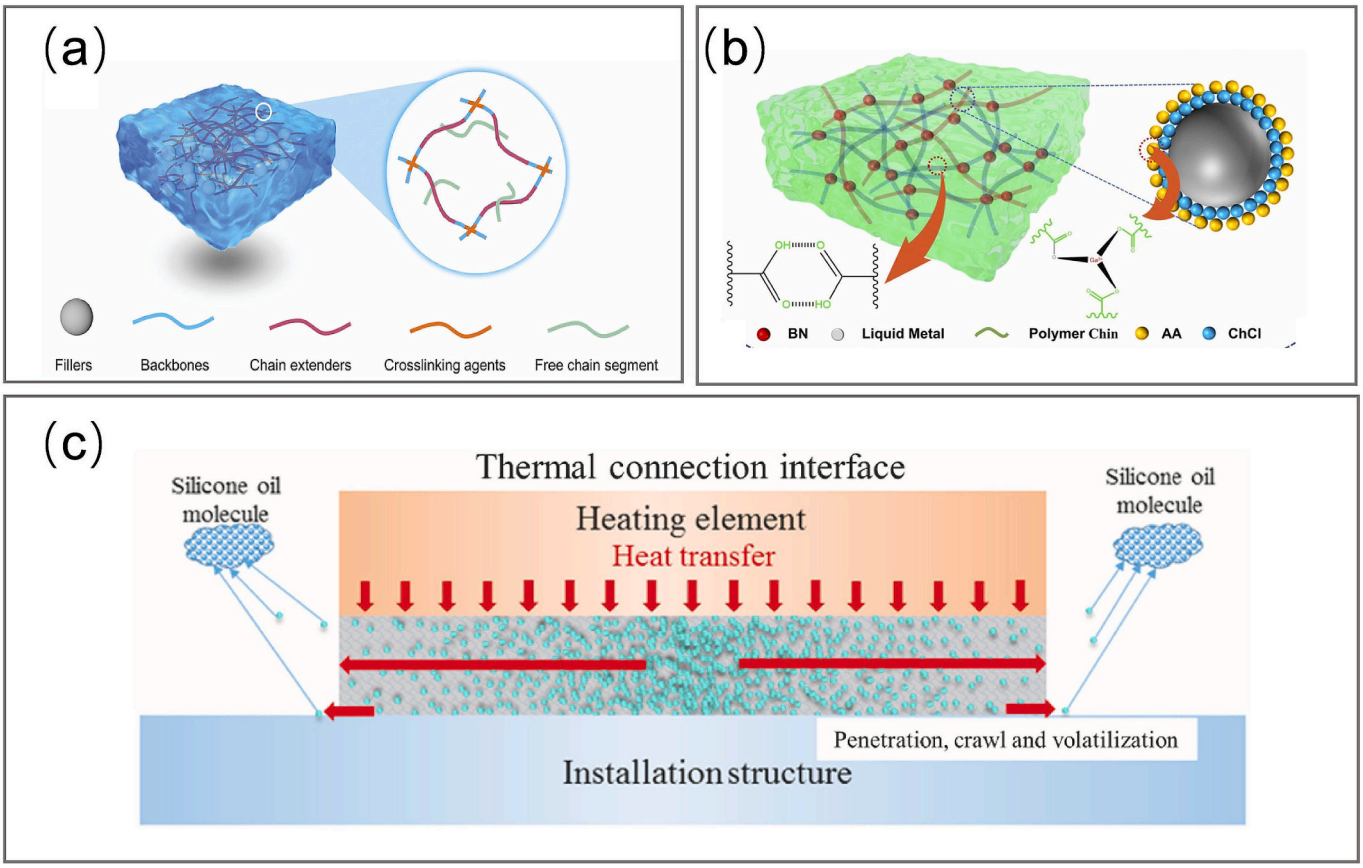

Fig. 6. Gel-type TIMs for gap filling, conformal contact, and long-term interfacial stability. (a) Schematic diagram of the soft composite gel-structure [16]. (b) Schematic diagram of the synthesis route of BN-PDES [104]. (c) Illustration of silicone oil loss in thermal grease [105].

composite gel [16], as illustrated in Fig. 6a, by lengthening the polymer strands between crosslinking points to improve compliance and using spherical Al fillers to establish thermal pathways. The resulting gel achieved a low thermal resistance of 0.14 cm^2 K W^{-1} at 10 psi. This design shows that the advantage of gel-type TIMs lies not only in softness, but also in the combination of conformal contact, thermal pathways, and mechanical retention. The same study also showed that further increasing filler content sharply raises viscosity, making the interfacial layer harder to compress and causing thermal resistance to increase again. Liu et al. prepared a BN-polymerizable deep eutectic solvent (PDES) gel through the synthesis route shown in Fig. 6b [104]. After spherical BN was introduced into the polymer gel network, increasing pressure reduced the material thickness and enlarged the contact area; the thermal contact resistance of 20 wt% BN-PDES decreased to 0.76 cm^2 K W^{-1} at 50 psi and remained stable during cycling tests. These results indicate that gel systems can provide pressure adaptability and cycling stability in addition to low thermal contact resistance, making them useful for interfaces with unfavorable geometric or assembly conditions.

For highly filled pastes and gels, yield stress, viscosity, and thixotropy influence spreading during assembly and the final BLT, so the gain in thermal conduction from additional fillers must be balanced against the loss of flowability. Excessive filler loading may cause hardening, aggregation, or restricted spreading, which can offset the benefit of higher thermal conductivity and raise contact thermal resistance again. The design target is therefore a balanced combination of thermal conduction, interfacial spreading, and flow restriction. Long-term reliability is a more prominent concern for conventional greases. Jiang et al. showed that silicone grease gradually loses silicone oil through penetration, crawling, and volatilization during service [105]. As illustrated in Fig. 6c, oil loss expands the dry region, disrupts filler connections, and lowers the effective thermal conductivity. For flowable TIMs, performance evaluation should therefore extend beyond the initial low-resistance state to the persistence of that state during long-term service.

5.3. *Liquid-metal-based TIMs*

Liquid metal (LM) and low-melting-point alloy (LMA) TIMs are typically described as high-thermal-conductivity systems. In gap-filling applications, however, their decisive function is to fill surface asperities and voids between the heat source, the TIM, and the heat sink by virtue of fluidity, deformability, and wettability. As TIMs transition from fundamental studies to practical use, bulk thermal conductivity should be assessed together with effective thermal resistance, BLT, interfacial stability, and encapsulation conditions [49,106,107]. Jia et al. reported a liquid metal–epoxy composite (LMEC) with the bulk thermal conductivity of 14 W m^{-1} K^{-1} at 85 vol% LM, while the lowest measured thermal resistance, 0.0043 K W^{-1}, occurs for the 65 vol% sample. In device heat-dissipation tests, the 65 vol% LMEC also outperforms indium foil, pure LM, the 85 vol% LMEC, and silicone-oil-based LM composites [106]. Luo et al. further show that the intrinsic thermal conductivity of LM is about 20 W m^{-1} K^{-1}, which is much lower than the 260–320 W m^{-1} K^{-1} reported for AlN, yet the thermal resistance of a silicone-oil/LM system is roughly five times lower than that of a silicone-oil/AlN system at the same volume fraction; this improvement is attributed to LM deformation and wetting at the interface [107]. Hence, evaluation of LM/LMA TIMs should move beyond a single *k* metric and emphasize effective thermal resistance and the true interfacial contact state [106,107]. From the constriction–spreading framework in Section 3.1, the principal contribution of liquid metal is to increase the size and number of effective heat-transfer contacts, thereby reducing the convergence and divergence of heat flow around isolated solid contact

spots. Its fluidity also addresses the multiscale gaps described in Section 3.3 by filling narrow asperity valleys and bridging larger terminal-height variations. This explains why liquid-metal-based interfaces can exhibit lower effective thermal resistance than solid fillers with higher intrinsic thermal conductivity, provided that wetting and confinement are adequately controlled.

This interfacial contact state is jointly governed by BLT, thixotropic rheology, surface wetting, and pressure-induced interface conformity. Mechanochemistry-mediated colloidal liquid metals reported by Wu et al. provide direct evidence for this mechanism. The Galinstan/AlN colloidal LM achieves a R_{EFF} of 0.42–0.86 mm^2 K W^{-1} in real thermal interfaces, owing to liquid–solid gradient heterointerface heat transfer and colloidal thixotropy [108]. In this system, AlN particles are stably dispersed in Galinstan, and mechanochemical reactions form an LM/AlN gradient heterointerface that promotes heat-carrier transport across the boundary (Fig. 7a(i)). The cream-state colloid spreads under pressure and remains stable after standing (Fig. 7a(ii)). At a Cu/Cu interface, the cream-state colloidal LM establishes intimate contact under 40 psi, leaving virtually no detectable air gap in the interfacial region (Fig. 7a (v)), and reduces the contact thermal resistance by 22-fold to 0.066 ± 0.020 mm^2 K W^{-1}. When the BLT approaches the scale of the largest filler, the effective thermal resistance at a BLT of 10 μm can be as low as 0.42 ± 0.077 mm^2 K W^{-1} (Fig. 7a(iii, iv)). At the device scale, this colloidal LM can bridge a 16 cm^2 heat source and, combined with microchannel cooling, extract 2760 W of heat. These results indicate that achieving a low R_{EFF} is more critical than a single high k for large-area, high-power thermal management [108].

At large-area interfaces, the low-resistance benefit of LM also requires that it connect discrete thermal pathways. Many high-k scaffolds or nanoarrays still make only point contacts and leave air gaps when their tips meet rough solid surfaces, so their bulk thermal conductivity does not translate into low effective interfacial resistance [11,109]. Liquid-bridging strategies restore continuity among separated solid heat-flow paths by introducing a flowable thermal-bridge phase. Cheng et al. fabricated a liquid-infused nanostructured composite comprising mechanically soft, thermally conductive double-sided Cu nanowire (CuNW) arrays and a tailored thermal-bridge liquid. Infusion of the liquid converts the original nanowire–surface point contact into a nanowire/liquid/surface composite contact and thereby markedly reduces contact thermal resistance [11] (Fig. 7b). When the scaffold is infused with liquid metal, the system achieves an interfacial thermal resistance of <1 mm^2 K W^{-1} in ASTM D5470 tests. By contrast, the bare CuNW scaffold exhibits a thermal resistance of 28.72 ± 1.14 mm^2 K W^{-1} at 100 psi, whereas liquid-infused nanostructured composite (LINC) lowers it to <1.0 mm^2 K W^{-1}. These observations indicate that, as a thermal-bridge liquid, the principal role of LM is to fill terminal gaps, replace air, and connect discrete thermal pathways.

LM can also activate terminal contact in oriented high-conductivity networks. Dai et al. developed a surface-metal-liquefaction graphene TIM that uses a three-layer design: vertically aligned graphene (VAGM) provides the high-k conductive scaffold, while surface metal liquefaction forms a flowable buffer at the graphene ends [109] (Fig. 7c). In the absence of LM, the VAGM surface comprises discretely distributed, height-irregular graphene edges that cannot deform sufficiently under conventional packaging pressure to conform to a rough heat-sink surface. As a result, micro- and nanoscale voids persist at the interface and the real contact area remains limited (Fig. 7c(i)). Multi-block lattice Boltzmann simulations further indicate that this discrete contact produces a pronounced temperature drop at the VAGM/heat-sink interface; the temperature difference between the lower VAGM surface and the upper heat-sink surface reaches 2.09 °C (Fig. 7c(ii)). Limited direct contact also yields a markedly nonuniform temperature distribution across the heat-sink upper surface (Fig. 7c(iii)). In LM-VAGM, a surface liquid metal layer fills the gaps between graphene ends and the rough heat sink, transforming the discrete graphene-edge/heat-sink contacts into a more continuous, LM-mediated interface (Fig. 7c(iv)). This modification reduces the interfacial temperature drop and homogenizes the heat-sink surface temperature distribution (Fig. 7c(v, vi)). The resulting structure attains a through-plane thermal conductivity up to 176 W m^{-1} K^{-1} and a two-sided contact thermal resistance as low as 4–6 mm^2 K W^{-1}. The LM buffer layer links vertical graphene to rough heat-source and heat-sink surfaces, increasing the effective contact thermal conductance by more than one order of magnitude. This approach differs from LINCs, in which a thermal-bridge liquid is infused into a nanowire scaffold to fill terminal voids; in LM-VAGM, surface metal liquefaction instead renders the ends of high-k vertical graphene conformable. Together, these studies demonstrate that LM can act as an interfacial thermal bridge between high-conductivity skeletons and rough solid surfaces.

However, LM does not inherently form an efficient thermal interface with solid surfaces. The high surface tension and native oxide of gallium (Ga) -based LM hinder wetting and spreading, and the thermal boundary resistance at the LM/solid interface can become a dominant contributor to R_C [110,111]. Zhang et al. examined how intermetallic compounds at Ga/Cu interfaces affect the thermal performance of LM TIMs. They reported that self-generated $CuGa_2$ lowers the thermal boundary resistance of liquid Ga/solid Cu interfaces from 1.11 × 10^{-7} m^2 K W^{-1} to 6.94 × 10^{-9} m^2 K W^{-1}, an approximately tenfold reduction [110]. This improvement reflects a change in interfacial bonding from van der Waals to metallic character and a shift in heat-carrier transport from phonon-dominated mechanisms to more efficient electron-mediated transfer. In chip tests, the interfacial temperature difference for the intermetallic-compound-assisted brushed LM was 10.2 °C, comparable to 8.3 °C for InSn solder and far lower than the 30.1 °C measured for conventionally oxidized LM [110]. These results indicate that LM flow–based gap filling must be integrated with interfacial chemistry and heat-carrier matching to approach solder-level interfacial heat transfer.

Leakage, electrical shorting, and long-term reliability remain central challenges for LM/LMA systems. Although pure LM offers low thermal resistance and excellent fluidity, its high mobility, metallic conductivity, and large surface tension promote leakage, electrical shorts, and poor spreading [99,111,112]. Consequently, practical applications typically require encapsulation, confinement, or blending with electrically insulating, high-k fillers. Jia et al. employed in situ curing of LM–epoxy composites to convert an amorphous, grease-like LM into a self-adaptive pad [9]. With an average LM droplet size of ~5–25 μm, a 70 vol% formulation exhibits a total thermal resistance of 2.19 mm^2 K W^{-1} and an adhesion strength of 0.497 MPa, while the cured morphology suppresses LM leakage [9]. These results imply that the low-resistance benefit of LM must be locked into shape-stable composite architectures [9].

Recent LM/diamond sandwich-structured TIMs exemplify this design logic: the gap-filling capacity of liquid metal must be transformed into a usable TIM by insulating encapsulation and interfacial reconstruction. Wang et al. constructed a diamond/liquid metal/epoxy (D/LM/EP) low-resistance encapsulation layer that exploits the synergy of micron-scale diamond, amorphous LM, and an epoxy matrix to isolate the LM into discrete microspheres embedded within the diamond/epoxy phase [112] (Fig. 7d(i)). In this arrangement, the LM bridges neighboring diamond particles and lowers local interfacial thermal resistance, while the diamond and epoxy interrupt continuous conductive LM pathways. The result is a dense, island-like microstructure that provides thermal-bridge connectivity while maintaining electrical insulation [112]. Applied to a rough LM@D substrate, the D/LM/EP layer acts as a low-resistance encapsulation layer on both faces, forming a sandwich architecture that integrates interface coating, core filling, and secondary encapsulation (Fig. 7d(ii)). The magnified image shows that D/LM/EP penetrates pores on the LM@D surface and fully fills submicron depressions, transforming the originally rough and potentially LM-exposed surface into a continuous, flat encapsulated interface (Fig. 7d(iii)). This D/LM/EP system attains a low thermal resistance of 4 mm^2 K W^{-1} at 40 psi, lowers the surface roughness to 0.29 ± 0.01 μm, corresponding to a

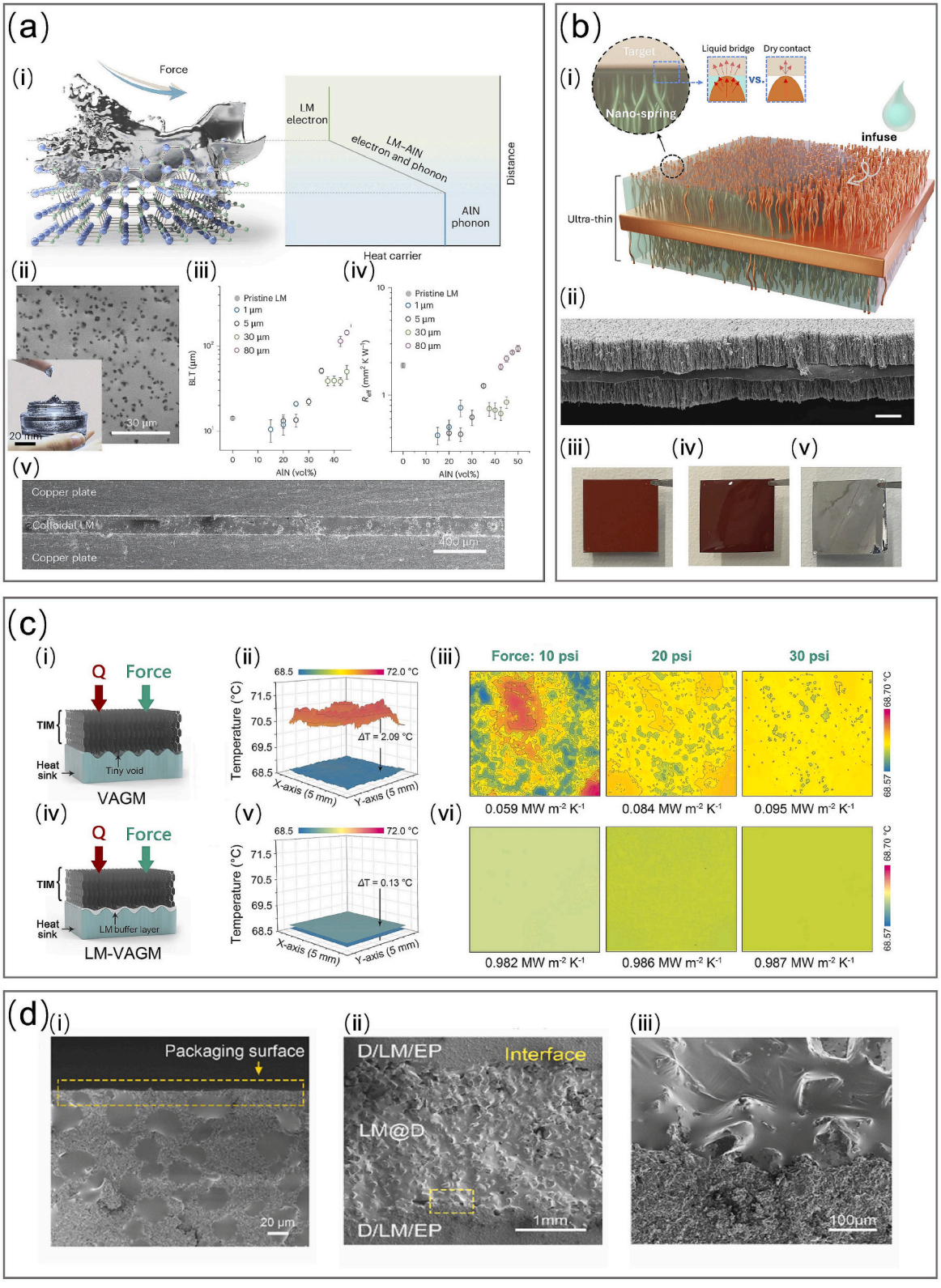

Fig. 7. Liquid-metal-mediated interfacial adaptation strategies for low-contact-resistance thermal interface materials. (a) Mechanochemically prepared liquid-metal/aluminum nitride (LM/AlN) colloids: (i) gradient AlN–LM heterointerface; (ii) SEM image of AlN particles dispersed in LM, with the inset showing the thixotropic colloidal LM; (iii, iv) BLT and effective thermal resistance as functions of AlN content and particle size; and (v) conformal contact of a cream-state colloidal LM between two Cu plates [108]. (b) Liquid-infused nanostructured composites (LINCs): (i) double-sided Cu nanowire (CuNW) scaffold infused with a thermal-bridge liquid; (ii) cross-sectional SEM image of the CuNW scaffold; and (iii–v) photographs of the CuNW scaffold, glycerol-LINC, and liquid-metal-LINC [11]. (c) Surface metal liquefaction of vertically aligned graphene TIMs: (i–iii) contact configuration, simulated interfacial temperature profile, and heat-sink surface temperature distribution for the vertically aligned graphene monolith (VAGM); and (iv–vi) the corresponding results for liquid-metal-modified VAGM (LM-VAGM) [109]. (d) Encapsulated LM/diamond sandwich TIM: (i) LM microspheres encapsulated within the diamond/LM/epoxy (D/LM/EP) layer; (ii) sandwich structure comprising D/LM/EP surface layers and an LM-coated diamond (LM@D) core; and (iii) enlarged interfacial morphology showing the filling of surface voids by D/LM/EP [112].

98.4% reduction relative to the LM@D substrate, and can fill surface pores up to 150 μm under applied stress. Concurrently, the external epoxy/diamond encapsulation and internal phase separation raise the volume resistivity to 2.25 × 10^{13} Ω cm, effectively preventing short circuits from exposed LM [112]. At a larger scale of thermal-network design, LM/diamond composites can form three-dimensional continuous thermal pathways via shear-induced Ga_2O_3 interfacial layers combined with gradient rotation-speed control, yielding an overall thermal conductivity of 237.9 W m^{-1} K^{-1}. Thus, the sandwich architecture confines the dynamic wetting and gap-filling behavior of LM within a secure encapsulated structure. The LM–diamond thermal bridge, the epoxy/diamond insulating layer, and the LM@D high-conductivity core act together to enable rough-interface filling, surface reconstruction, low contact thermal resistance, and electrical safety.

In summary, researchers have pursued several strategies to overcome the challenges of converting high κ into low R_{EFF}, addressing point contact at rough interfaces, LM leakage and shorting, and dynamic interfacial instability in LM/LMA TIMs. Galinstan/AlN colloidal LM [108] lowers R_{EFF} across large-area real interfaces by combining gradient liquid–solid heterointerfaces with thixotropic behavior. Liquid-infused CuNW composites [11] and surface-metal-liquefaction graphene TIMs [109] create continuous thermal pathways by using liquid bridges to join discrete high-k skeletons. Ga/Cu intermetallic compound interfaces [110] decrease thermal boundary resistance via interfacial reactions. D/LM/EP sandwich structures [112] pair insulating encapsulation with diamond networks and dynamic LM wetting to yield low thermal resistance while maintaining electrical safety. Together, these approaches illustrate a common design principle: the performance of LM/LMA TIMs derives chiefly from the synergy of flow-based gap filling, interfacial wetting, thermal-bridge formation, and confined stability, rather than from the intrinsic high thermal conductivity of the metallic phase alone.

6. Structured TIMs for low contact thermal resistance

Beyond flexible matrices, adaptive interfaces, and gap-filling media, structural design also targets the construction of internal heat-flow pathways in TIMs. Randomly dispersed fillers raise composite thermal conductivity, but contacts between fillers often remain discontinuous. Because heat must repeatedly traverse the polymer phase and filler–filler interfaces, bulk thermal resistance is difficult to minimize [113,114]. Constructing continuous thermal networks arranges high-*k* fillers such as BN, graphene, CNTs, CuNWs, or graphite into through-plane, in-plane/through-plane coupled, or three-dimensional heat-flow pathways, thereby enhancing internal heat-transfer efficiency [25,27,115]. Structured thermal pathways, however, introduce new interfacial challenges. When the ends of vertical sheets, nanowire arrays, or carbon-based skeletons cannot effectively reach heat-source or heat-sink surfaces, terminal contact insufficiency, limited interfacial coupling, and local air gaps still occur. Moreover, highly oriented or high-density networks can increase local stiffness and reduce the material's ability to conform to rough interfaces [16,31,88,116]. Thus, structured TIMs with low contact thermal resistance must address two issues at once: continuity of internal thermal paths and effective external interfacial access. This section first examines how continuous thermal networks establish low-resistance heat-flow channels and cut terminal heat-transfer losses. It then analyzes how compressible structures, micro-protrusions, and flexible ends enlarge real contact area and relieve interfacial mismatch induced by structural rigidity.

6.1. TIMs with continuous thermal networks

Continuous thermal networks serve primarily to link discrete fillers into through-plane, coupled in-plane/through-plane, or fully three-dimensional heat-flow pathways, thereby reducing internal thermal resistance in TIMs. Examples such as BN/graphite oriented pathways [82], graphene-fiber vertical arrays [23], graphite/silicone through-plane channels [117], CNT-encapsulated arrays [91,118], and CuNW/3D graphene sandwich structures [116] demonstrate that high-*k* fillers markedly enhance directional heat transfer only when organized into continuous pathways. However, internal network continuity does not automatically produce a corresponding drop in total thermal resistance. Effective access of network termini to the heat-source or heat-sink surfaces remains constrained by terminal contact, interfacial coupling, assembly pressure, and BLT [23,91,116–118]. Therefore, the central question addressed in this section is how continuous thermal pathways can be extended from the material interior to the external contact interface. As described by the constriction–spreading model in Section 3, discrete terminal contacts force heat flow to converge into small contact regions and then spread into the substrate, producing additional interfacial resistance. Surface caps, arc-like bridges, liquid interlayers, and horizontal outlet layers reduce this resistance by enlarging the effective terminal contact area and improving the continuity between internal thermal pathways and the external substrate.

In electrically insulating TIMs, BN networks most commonly form continuous through-plane pathways. Stacked-and-cut BN/graphite layered silicone rubber [82] preserves the high orientation of BN and graphite films, enabling rapid through-plane heat flow. Shear-oriented, layer-by-layer stacked BN/silicone rubber composites [80] enhance through-plane conduction by aligning BN flakes and forming percolating networks, while retaining flexibility and elastic recovery. Large-scale BNNS/PDMS systems [81] produce high-quality BN nanosheets by high-power ultrasonication and then construct through-plane heat-transfer paths via multistage casting, yielding low interfacial thermal resistance and a low dielectric constant. BN structures fabricated through rolling, curing, cold pressing, and vertical cutting further transform BN sheet alignment into low-modulus through-plane channels [119]. BN systems combine electrical insulation, thermal stability, and good processability; however, when vertical nanosheet edges contact the heat-source or heat-sink surfaces, phonon reflection and insufficient interfacial coupling can still occur. Thus, the design of the terminal heat-flow outlet requires special attention.

Zhan et al. further demonstrated this terminal-coupling concept with an interfacial arc-like phonon bridge [120] (Fig. 8a). Using stacking and cutting to fabricate BNNS-TIMs, the method produces vertically aligned BNNS layers at the film center that provide through-plane heat-flow pathways. Concurrently, shear during cutting generates an ultrathin, horizontally aligned BNNS layer on the top and bottom cut surfaces, creating an arc-like transition between the vertical thermal pathways and the external contact interface [120] (Fig. 8a(i)). SEM images confirm this alignment: BNNS in the bulk region are predominantly perpendicular to the film surface (Fig. 8a(ii)), whereas a horizontal BNNS layer appears at the machined surface (Fig. 8a(iii)). In side-view images near the cut surface, the 50 wt% sample exhibits pronounced BNNS rotation, whereas this rotation is markedly weakened in the 90 wt % sample, indicating that filler loading influences the formation of the near-surface arc-like alignment (Fig. 8a(iv, v)). X-ray diffraction (XRD) data corroborate this observation by showing reduced near-surface BNNS rotation at high filler loading. The arc-like transition between the bulk vertical layer and the surface horizontal layer diminishes phonon back-reflection at the interface and improves phonon coupling efficiency. Consequently, the thermal contact resistance of the BNNS composite film decreases by 70% to 0.059 in^2 K W^{-1}. These results imply that terminal design in electrically insulating continuous networks must address both bulk through-plane heat transfer and near-surface phonon bridging; merely increasing the vertical orientation of BNNS is insufficient to fully lower interfacial thermal resistance.

Carbon-based continuous networks further raise the upper limit of thermal conductivity. Vertically assembled functionalized multilayer graphene [121] exploits the high in-plane conductivity of functionalized multilayer graphene sheets (fMGs) and vertical stacking to create a graphene-based TIM architecture. Dual-field–aligned graphene-fiber

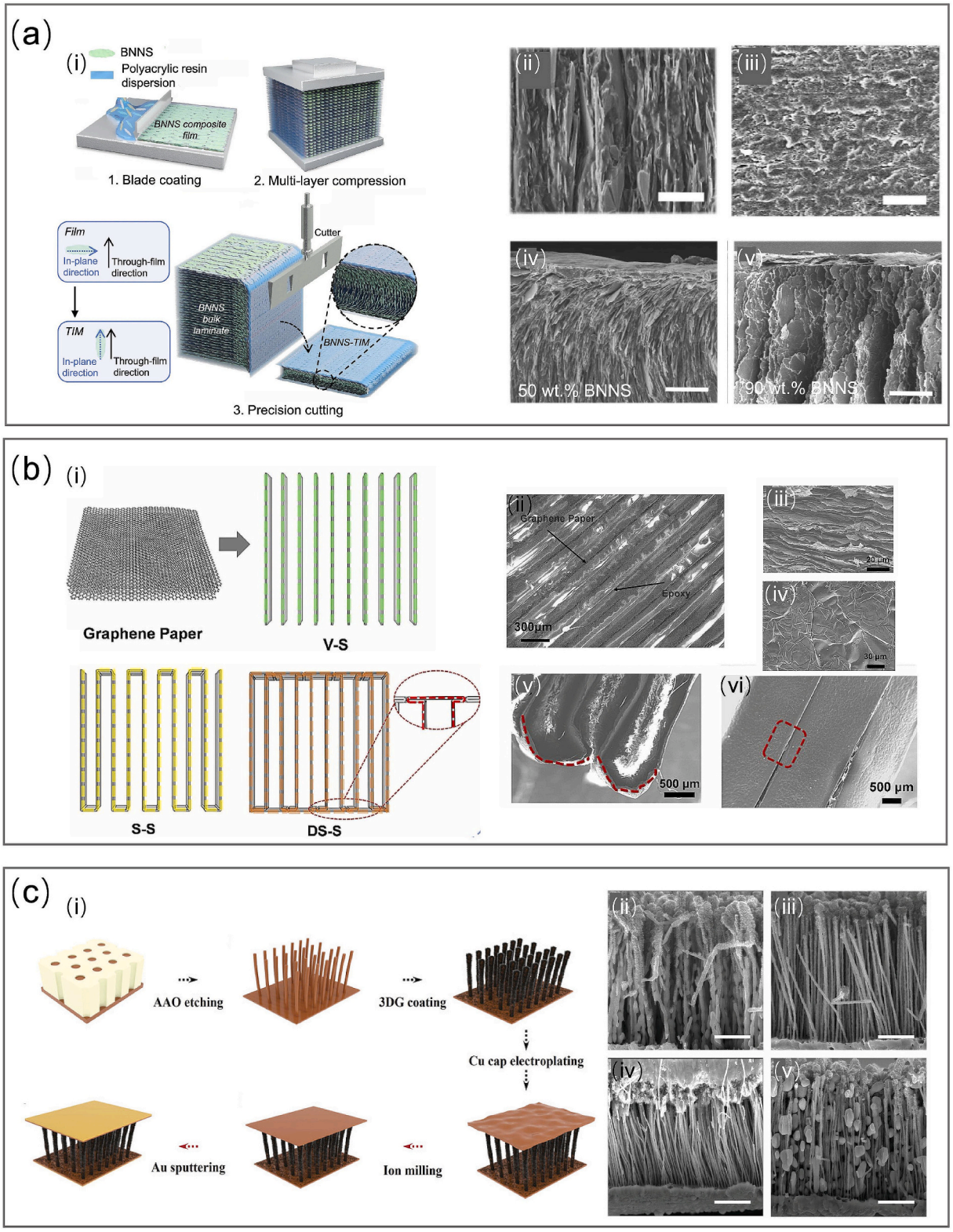

Fig. 8. Continuous thermal networks with engineered pathways to the external interfaces of structured thermal interface materials. (a) Interfacial arc-like phonon bridges in boron nitride nanosheet (BNNS)-based TIMs: (i) stacking–cutting fabrication and the resulting BNNS arrangement; (ii) vertically aligned BNNSs in the bulk; (iii) horizontally aligned BNNSs at the machined surface; and (iv, v) near-surface BNNS arrangements at filler loadings of 50 and 90 wt%, respectively [120]. (b) Continuous graphene-film (GF)/polymer square-wave-like thermal networks: (i) vertical (V—S), square-wave-like (S—S), and double square-wave-like (DS-S) structures; (ii) cross-sectional morphology of the GF/polymer composite; (iii, iv) layered morphology of the GF; (v) continuous GF at the turning point of the S—S structure; and (vi) top-view morphology of the DS-S surface [40]. (c) Cu-capped three-dimensional graphene/copper nanowire (3DG-CuNW) sandwich TIM: (i) fabrication of the sandwich structure and preparation of the specimen for frequency-domain thermoreflectance measurement; (ii, iii) 3DG-CuNW arrays prepared by plasma-enhanced chemical vapor deposition at 600 and 500 °C, respectively; (iv) cross-sectional morphology of the Cu-capped sandwich TIM; and (v) Sn infiltration into an uncapped CuNW array during electrochemical deposition [116].

TIMs [23] employ mechanical–electric dual-field synergistic alignment to orient graphene fibers vertically and establish dense through-plane heat pathways. Vertical graphite/silicone pads [117] transform low-cost graphite sheets into vertical thermal channels, combining high through-plane conductivity with mechanical softness. VACNT/horizontal graphene-film orthogonal three-dimensional hybrid networks [25] build multiscale heat-flow pathways by pairing vertical CNTs with horizontal graphene films. Such carbon-based networks can markedly enhance through-plane or bidirectional heat transfer. However, the terminal ends of highly oriented graphene, graphite, or CNT structures are often discretely distributed, and height mismatch together with limited contact area at these ends restricts heat injection from the heat source or heat sink into the high-*k* (networks)

To overcome the discrete surface distribution and limited effective contact area of vertical graphene channels, Xu et al. introduced graphene film (GF)/polymer square-wave-like composites [40] (Fig. 8b). In the conventional vertical structure (V—S), aligned graphene sheets use graphene's high in-plane thermal conductivity to create through-plane heat pathways, but the high-*k* channels are exposed only at the cross section while the surface remains partly covered by polymer. This configuration restricts direct contact between hot spots and the vertical pathways. To enhance terminal contact, the authors exploited the flexibility and foldability of graphene films to transform the V—S into a square-wave–like structure (S—S). By applying extrusion bending, they produced a double square-wave-like structure (DS-S), which extends the high-*k* graphene film skeleton from isolated vertical channels into a continuous architecture that combines vertical heat-flow pathways with horizontal contact surfaces (Fig. 8b(i)). Structural characterization confirms the continuity of the GF skeleton and the terminal planarization effect. The GF/PET cross section exhibits a continuous layered architecture with no obvious cracks between the PET film and dense GF (Fig. 8b(ii)). The anisotropic layered stacking of GF underlies rapid in-plane heat transfer (Fig. 8b(iii, iv)). In S—S, GF remains continuous at the turning point, indicating that folding does not disrupt the heat-flow path (Fig. 8b(v)). After forming DS-S, adjacent GF regions make close contact at the top and partially cover the polymer cross section, generating a more continuous, high-*k* horizontal contact surface (Fig. 8b(vi)). This combination of vertical channels and horizontal high-*k* contact surfaces yields DS-S a thermal conductivity of 60.56 W m^{-1} K^{-1} and reduces R_C by about 30% relative to S—S. The result indicates that carbon-based continuous networks must convert discrete vertical channels into accessible horizontal heat-flow outlets to more effectively lower contact thermal resistance.

Continuous networks formed from nanowire arrays still face challenges in terminal protection and reliable terminal connection. Bare vertical nanowires combine high axial thermal conductivity with good mechanical compliance, but they are prone to collapse, oxidation, and infiltration by solder during assembly; free-end contacts can also add interfacial thermal resistance [91,116]. Jing et al. addressed these issues by fabricating a sandwich-structured flexible TIM that uses vertically aligned CuNW arrays as the core thermal pathway [116]. Their process comprises CuNW electrodeposition on a copper-coated anodic aluminum oxide (AAO) template, wet etching to release a free-standing CuNW array, low-temperature plasma-enhanced chemical vapor deposition (PECVD) of 3D graphene, addition of upper and lower Cu cap layers to form the sandwich, and ion milling followed by Au transducer deposition for frequency-domain thermoreflectance (FDTR) thermal characterization (Fig. 8c(i)). The high aspect ratio of the CuNWs imparts mechanical compliance, and the 3D graphene (3DG) coating supplies extra thermal pathways while protecting the CuNWs from oxidation. Temperature control during 3DG coating is critical for preserving structural integrity. SEM images show that PECVD at 600 °C induces partial fusion of CuNWs, whereas PECVD at 500 °C preserves the CuNW array morphology and yields a more uniform 3DG coating (Fig. 8c(ii, iii)). In the resulting sandwich TIM, the thin Cu layers above and below make intimate contact with the 3DG-CuNW tips, converting a potentially weak graphene–metal terminal into a robust metal–metal junction and shielding the nanowire array during subsequent assembly (Fig. 8c(iv)). Without this Cu cap, Sn infiltrates the CuNW gaps during electroplating or bonding, solidifies into particles, and disrupts the array structure and terminal heat-transfer pathways (Fig. 8c(v)). Thus, the Cu cap functions both as a thermally conductive contact and as a mechanical protection layer for device integration. Because the CuNW/3DG core connects with the upper and lower Cu layers with low electrical and thermal resistance, the sandwich TIM achieves an overall thermal resistance as low as about 0.23 mm^2 K W^{-1} while retaining good flexibility. This finding indicates that the performance limits of continuous nanowire networks typically stem from terminal contacts, assembly protection, and interfacial connections, rather than from the intrinsic thermal conductivity of individual nanowires alone [116].

CNT arrays face a common challenge in converting their high axial thermal conductivity into effective interfacial heat transfer. Cu-VACNTs-Cu sandwich TIMs [91] employ a transfer-and-encapsulate strategy and a two-step soldering process to embed both VACNT ends in Cu microfoils, thus avoiding direct VACNT growth on the chip die and reducing free-end contact resistance. CNT/ polyphenylene sulfide (PPS)/CNT film-type TIMs [118] create a stable solid-state interface by combining two opposing CNT forests with an intermediate PPS film, and experiments indicate that interfacial contact thermal resistance dominates the total thermal resistance. Al-capped CNT forests [122] introduce an Al cap as a phonon-bridging layer to enhance phonon–electron coupling between CNTs and metal heat sinks. Together, these studies demonstrate that metal capping, flexible interlayers, or bridging layers are required to convert CNT arrays' intrinsic axial conductivity into practical interfacial heat transfer [91,118,122].

In summary, researchers have developed multiple continuous thermal-path designs to overcome discontinuous heat-flow paths in dispersed fillers, inadequate terminal contact in oriented networks, and limited interfacial coupling of high-*k* skeletons. BN/graphite stacked-and-cut structures [82], BN/silicone rubber shear-oriented structures [80], large-scale BNNS/PDMS multistage casting structures [81], and rolled-vertically cut BN structures [119] primarily enhance electrically insulating through-plane heat transfer. Arc-like BNNS phonon bridges [120] further reduce phonon reflection and contact thermal resistance at BN network terminals. Graphene square-wave-like structures [40] link discrete vertical channels via continuous high-*k* horizontal planes. CuNW/3DG sandwich TIMs [116] protect nanowire terminals and connect them through upper and lower Cu layers. Cu-VACNTs-Cu [91], Al-capped CNT forests [122], and CNT/PPS/CNT films [118] lower CNT terminal thermal resistance by encapsulation or bridging layers. An effective continuous-thermal-network design must therefore achieve three concurrent goals: establish low-resistance heat-flow paths within the material, provide terminal heat-flow outlets that access external interfaces, and preserve interfacial-coupling stability during assembly and service.

6.2. *Compressible TIMs for enlarged real contact area*

Continuous thermal networks describe heat-flow pathways within materials, but high-conductivity architectures achieve low contact thermal resistance only when they conform to rough mating surfaces under assembly load. For solid or semi-solid TIMs, the relevant variables extend beyond *k*; they also include compression response, BLT, surface morphology, recovery stability, and real contact area. High-modulus networks preserve continuity of thermal pathways yet can leave air gaps at the interface. By contrast, architectures with compressible bodies and deformable termini conform more readily to heat-source and heat-sink surfaces under applied pressure. The pressure response of compressible TIMs is directly consistent with the CMY and Mikic models: lowering effective hardness or elastic modulus increases deformation and real contact area under a given assembly pressure [69,70]. However, because practical surfaces contain roughness across

multiple length scales, the M–T fractal model and the Clausing–Chao two-scale description are also relevant. Compressible bodies accommodate macroscopic waviness, whereas deformable micro-protrusions and soft terminals engage smaller asperities [76,77]. Structural compliance therefore reduces contact resistance only when deformation occurs hierarchically across both bulk and surface length scales.

Pressure response first appears as BLT compression and improved terminal conformity. Lightweight vertical graphene foams remain soft and compressible at low filler loadings, which optimizes through-plane heat conduction while reducing contact thermal resistance [123].

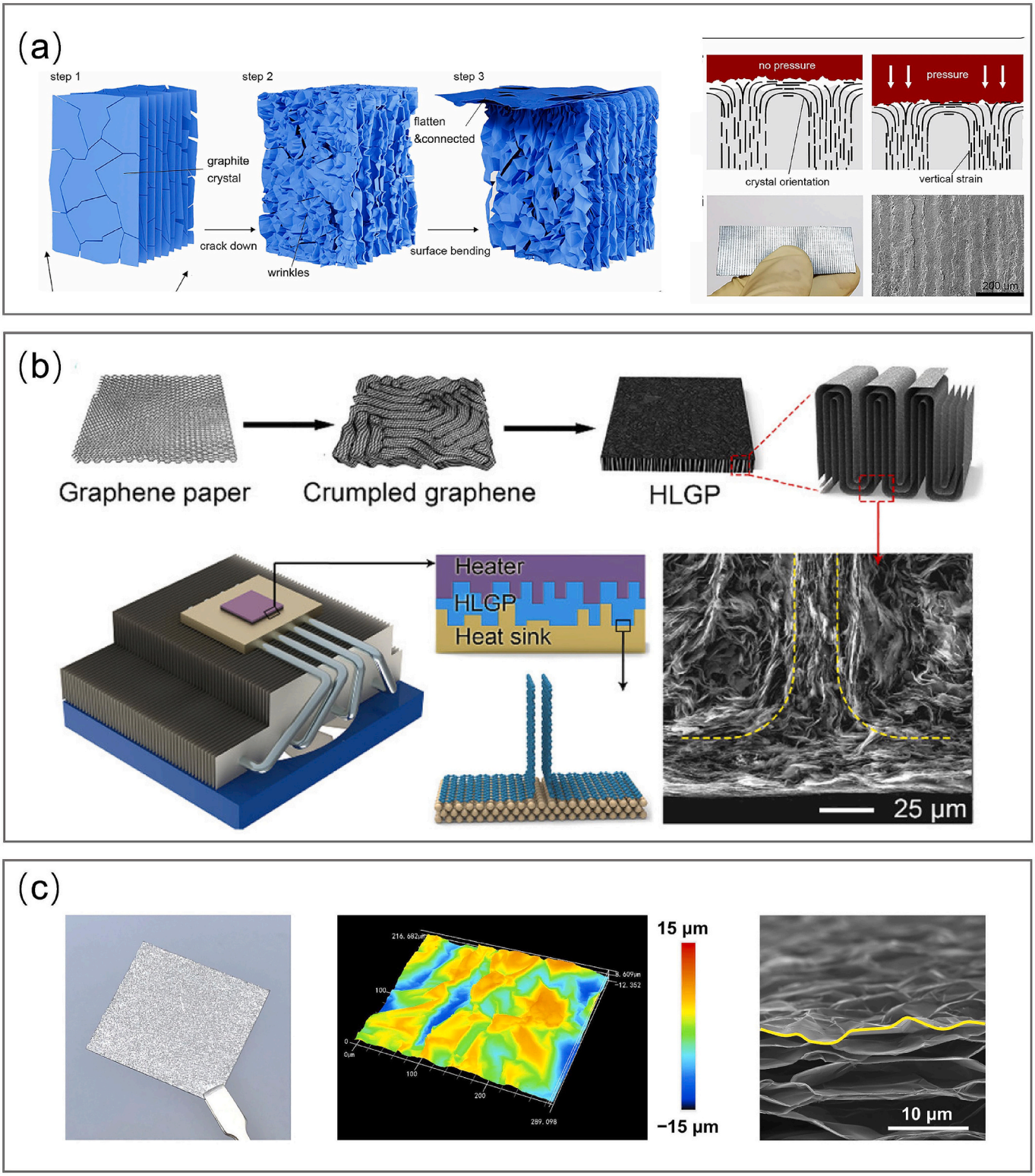

Fig. 9. Compressible solid TIMs for enhanced real contact area and low thermal resistance. (a) In situ graphite cracking and surface polishing for compressible carbon–silicone thermal pads [38]. (b) Honeycomb panel-like graphene pad with vertical heat pathways and compliant surface contact [125]. (c) Surface-bulged graphene-lamellae network for conformal solid TIMs [37].

Ultrathin all-carbon graphene foams demonstrate that increased assembly pressure can significantly compress the BLT and convert a high-conductivity foam into a thinner interfacial layer [124]. In carbon–silicone composite pads, in situ graphite cracking combined with precision mechanical polishing produces smooth interfaces and deformable graphite structures, yielding high bulk thermal conductivity, large compressive strain, and ultralow total thermal resistance simultaneously [38]. As illustrated in Fig. 9a, Luo et al. used ultrasonic treatment to crack and loosen vertically oriented graphite flakes embedded in a silicone gel matrix, then applied polishing to interconnect the surface graphite layers [38]. After treatment, the graphite structure compresses more vertically, while the polished surface forms horizontally connected graphite pathways that spread heat near the interface. This two-step treatment therefore links bulk compressibility with surface contact integrity, allowing the carbon–silicone pad to reach a total thermal resistance of 1.8 $mm^2\ K\ W^{-1}$ at 50 psi and a compressive strain of 45% at the same pressure.

Dai et al. developed a honeycomb panel-like graphene pad (HLGP) by mechanically processing graphene paper [125]. The resulting hierarchical structure contains vertically aligned graphene in the interior and thin horizontally oriented graphene caps on both surfaces (Fig. 9b). The vertical graphene framework provides a through-plane thermal pathway, whereas the horizontal caps act as terminal heat-spreading layers that improve contact with the heater and heat sink. This structure allows the pad to deform under packaging pressure while retaining efficient heat transport. More importantly, after removing the horizontal caps, the through-plane thermal conductivity increases to 176 $W\ m^{-1}\ K^{-1}$, but the contact thermal resistance rises from 5.8 to 22.0 $mm^2\ K\ W^{-1}$, showing that terminal conformity and surface heat spreading can be more decisive than bulk conductivity alone for reducing contact thermal resistance.

Terminal and surface geometry can further increase the real contact area. Huang et al. added abundant micro-protrusions to a three-dimensional interconnected graphene lamellae network, which allows the solid TIM to better conform to varied substrate morphologies under pressure and enhances through-plane heat transfer during network deformation [37]. As shown in Fig. 9c, their surface-bulged graphene-lamellae network (SBGLN) presents a metallic-luster solid pad, a rough micro-bulged surface, and a porous lamellar cross-section. According to the original work, these micro-bulges have lateral sizes of 20–80 μm and heights of 5–15 μm, and the pores between adjacent graphene lamellae have an average size of about 16.7 μm. This structure gives the solid TIM two interface-relevant functions: the surface micro-bulges deform to match rough substrates, and the porous lamellae network provides compressibility for BLT reduction under pressure. In BN systems, non-solvent-induced phase separation combined with in situ welding produces finger-like continuous BN skeletons, while a silicone rubber matrix supplies compressibility and conformity so the film maintains low contact thermal resistance across different pressures [126]. Tian et al. engineered the ends of vertical graphene so that, after silver-paste shrinkage, exposed soft GF tips form a deformable surface that lowers contact thermal resistance while preserving high through-plane thermal conductivity [127]. Cocklebur-inspired PUC composites employ protruding surfaces and bark-like interlocking structures to anchor functional particles, enabling surface morphology and internal particle networks to work together to reduce interfacial thermal resistance. Together, these studies indicate that structural terminals should not be treated merely as endpoints of high-conductivity networks; they should be designed as functional interfaces that deform, conform, and enlarge the real contact area.

Design of compressible structures is being extended to dynamic and non-flat interfaces. He et al. developed dandelion-inspired radial graphene/LM microspheres [128]. A radial graphene framework confines and supports LM, while an Ecoflex matrix accommodates large deformations. Together, these components form recoverable, anti-leakage hybrid liquid metal/graphene microspheres/Ecoflex composites (HLMGS/E composites). Its low compressive modulus and high recovery preserve conformal contact under vibration and irregular interfaces, resulting in low contact thermal resistance. Crucially, HLMGS/E retains high thickness recovery and shows minimal thermal-conductivity decay after 100 cycles at 40% compression, indicating that real contact area must be established at initial pressure and preserved after cyclic deformation. This work indicates that TIM interfacial design should address not only the contact state under assembly pressure but also retention of real contact area under vibration, morphology changes, and cyclic loading.

6.3. Comparison of R_C among different TIM types

To establish a comparative framework for different types of TIMs, Fig. 10 summarizes the literature-reported area-normalized R_C values of polymer composite TIMs, structured TIMs, gel/grease TIMs, liquid-metal (LM) TIMs, and phase-change-material (PCM) TIMs. The data are plotted on a logarithmic scale and further distinguished by the applied pressure, including $p \leq 10$ psi, $10 < p \leq 100$ psi, and $p > 100$ psi. Horizontal brackets connect multiple values reported in the same study or for the same material under different testing conditions.

As shown in Fig. 10, the reported R_C values span several orders of magnitude and overlap substantially among different TIM types. LM TIMs generally exhibit relatively low R_C because their fluidity and interfacial wettability facilitate conformal contact and gap filling. Gel/grease TIMs also rely on flow-assisted filling of surface asperities, but their reported values cover a broad range because of differences in composition, bond-line thickness, and applied pressure. PCM TIMs reduce R_C through thermally induced softening or melting, whereas polymer composite TIMs mainly depend on matrix compliance and filler-network design to balance bulk thermal transport and interfacial conformity. Structured TIMs improve interfacial heat transfer by extending aligned or interconnected thermal pathways toward the external contact surfaces. Nevertheless, the considerable overlap among these types indicates that the TIM classification alone does not determine R_C; material formulation, interface design, and testing conditions are equally important.

Accordingly, reported contact thermal resistance values should be interpreted together with their measurement conditions. Applied pressure, substrate material and surface roughness, contact area, bond-line thickness, test temperature, and measurement method or standard can all affect the measured value. For example, results obtained using copper fixtures may not accurately represent the contact behavior of a TIM on silicon surfaces, because the two substrates differ in surface chemistry, hardness, roughness, and deformation behavior. In addition, steady-state and transient methods may probe or combine different components of the overall thermal resistance, depending on the experimental configuration and data-reduction procedure. Values reported under different test conditions should therefore not be directly compared unless these parameters are clearly specified.

7. Summary and outlook

Future research on TIMs should move from simply increasing intrinsic thermal conductivity to building interface engineering systems that can adapt to real engineering surfaces. The current challenge is no longer limited to showing very high thermal conductivity under ideal test conditions. More importantly, TIMs must form close and stable heat transfer paths when they contact rough, warped, or dynamically changing device surfaces. Therefore, the ability to fill interfacial gaps should be evaluated together with BLT, pressure response, surface wetting, and long-term interfacial stability. This change in perspective means that TIM performance should not be judged as an isolated material property. Instead, TIMs should be viewed as part of the whole package, with emphasis on their ability to maintain efficient thermal coupling under complex service conditions. This view is closer to the

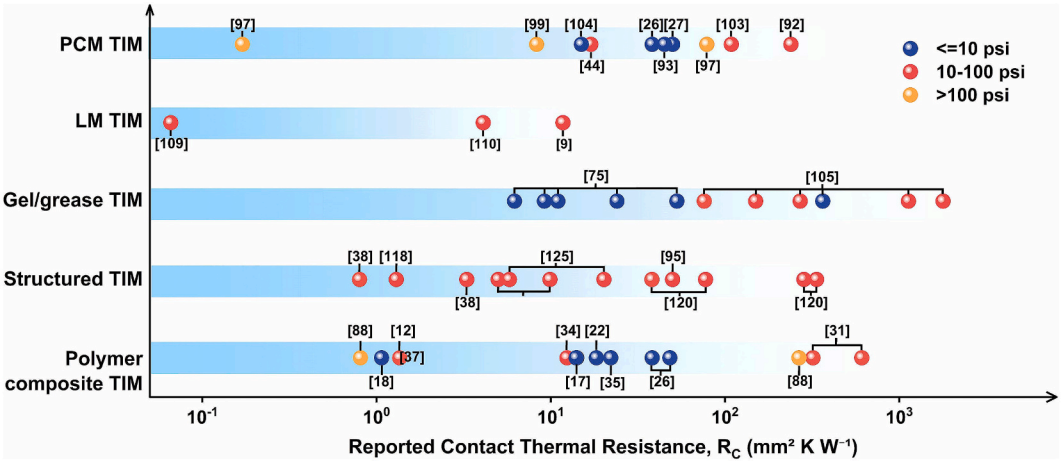

Fig. 10. Comparison of literature-reported area-normalized contact thermal resistance values among different types of thermal interface materials.

real needs of electronic packaging for reliability and heat dissipation.

For current strategies that aim to improve thermal conductivity, future studies should focus on the coupling between intrinsic thermal networks and interfacial compliance. These two factors should not be treated only as competing requirements. For example, in highly filled polymer composites, simply increasing filler content often increases stiffness and worsens interfacial contact. By controlling filler shape, particle size distribution, and surface modification, it is possible to maintain effective heat transfer pathways while improving rheology and promoting the filling of microscopic gaps. For materials with vertically aligned thermal networks, the coupling between network ends and the external interface needs more attention. Liquid metals or soft polymer modification layers can be introduced to preserve internal thermal continuity while giving the surface enough deformability. Such targeted structural design aims to improve both thermal conduction and contact adaptation, rather than making a simple trade-off between them. Over the next 3–5 years, TIM research should prioritize materials that combine high through-plane thermal conductivity, low modulus, and stable interfacial contact. Promising directions include soft polymer matrices with suppressed oil bleeding, hierarchical filler packing, surface-energy matching, dynamic covalent polymer networks, and encapsulated liquid-metal systems. These strategies should be integrated with scalable processing methods to maintain low BLT and low contact thermal resistance over large or uneven interfaces. A major breakthrough may come from TIMs that preserve both continuous thermal pathways and conformal contact during thermal cycling and mechanical vibration.

To achieve this goal, intelligent interface structures with dynamic response will become an important direction. An ideal TIM should be able to deform locally, reconstruct through limited flow, or exchange dynamic bonds at the contact region. These responses help the material wrap surface asperities and remove trapped air, while maintaining the integrity of the whole structure at the macroscopic scale. Soft polymer networks, phase-change components, and deformable terminal structures should not be viewed only as mechanical modification methods. They are key ways to increase interfacial compliance, maximize real contact area, replace trapped air, and reduce the high thermal resistance caused by microscopic voids. Future structural design must optimize internal heat transfer networks and interfacial contact at the same time. Only when the ends of aligned fillers or porous skeletons can effectively couple with the heat source and heat sink can the internal thermal network have real engineering value. Therefore, terminal compliance and interfacial adhesion should be considered from the beginning of TIM structural design. Artificial intelligence and machine learning may further accelerate TIM design. By correlating composition, filler architecture, rheological properties, modulus, surface roughness, assembly pressure, BLT, and thermal resistance, data-driven models can identify relationships that are difficult to isolate through single-variable experiments. Multi-objective optimization can be used to balance thermal conductivity, contact thermal resistance, processability, and reliability. Physics-informed models may further predict interfacial contact and thermal transport under specific surface and loading conditions. However, these approaches require standardized datasets with consistent test conditions and reliability data.

Beyond material-level optimization, future TIMs should be integrated with complementary thermal-management technologies, including passive thermal regulation, microchannel cooling, programmable thermal pathways, and thermophotovoltaic heat recovery [129–132]. Such system-level integration may enable more efficient and comprehensive thermal management for next-generation electronic devices.

The evaluation system also needs to change so that it can reflect performance under real service conditions. Bulk thermal conductivity alone is no longer enough to judge the value of TIMs. Future TIM studies should report effective thermal resistance together with the conditions that determine it, including BLT, applied pressure, substrate material and roughness, contact area, and test temperature. Long-term tests should also specify the temperature range and number of thermal cycles and, where relevant, quantify pump-out or dry-out. Interfacial morphology after aging should be examined to determine whether the increase in thermal resistance is caused by damage to the internal thermal network or by loss of contact between the TIM and the substrate. Reporting these parameters as a minimum set would improve the comparability of different studies and provide a clearer link between material properties and performance in practical packages. Test conditions should simulate real device geometry, temperature gradients, and long-term operation, so that failure mechanisms at dynamic interfaces can be identified. Without these practical tests, reported high thermal conductivity may not translate into efficient heat dissipation in real packages. By building a multidimensional evaluation system that includes interface morphology, contact mechanics, and thermal reliability, researchers can more accurately identify the key factors that control contact thermal resistance. This will guide the rational design of next-generation TIMs with low contact thermal resistance. New in-situ characterization methods are also needed to track the evolution of TIM interfaces during assembly and service. Imaging of the real contact area can reveal changes in interfacial contact, micro-computed tomography can identify internal pores and filler distributions, pressure mapping can measure local contact pressure, and spatially resolved thermal measurements can locate high-resistance regions. Combining these methods under controlled pressure, temperature, and cyclic loading can directly correlate interfacial morphology with thermal

resistance. Such multimodal characterization can determine whether performance degradation originates from disruption of the internal thermal network or loss of TIM–substrate contact.

In summary, the next breakthrough in flexible TIMs should come from moving beyond the assumption that high thermal conductivity must come at the cost of poor contact performance. Future TIMs should be multifunctional material systems that combine high bulk heat conduction with excellent interfacial adaptation. This requires a deeper understanding of the coupling among filler network construction, interfacial wetting, and stress transfer. Through the combined optimization of microstructure design and surface engineering, TIM development can move from material properties to system-level performance. The future standard for success should be the ability of a TIM to maintain low contact thermal resistance and high heat flux transfer on real, complex, and dynamically changing interfaces. This interface-centered research direction will help move TIM technology from ideal laboratory demonstrations toward engineering applications that meet the strict requirements of high- performance electronic packaging. Ultimately, it will improve the thermal management efficiency and reliability of the whole electronic system.

Declaration of competing interest

The authors declare that they have no known competing financial interests or personal relationships that could have appeared to influence the work reported in this paper.

Acknowledgments

This work was funded by Shenzhen Municipal Key Industrial Research and Development Program (ZDCY20250904161859001), National Natural Science Foundation of China (22475007), MIND project (MINDKT202504).

Data availability

No data was used for the research described in the article.

References

[1] S. Xu, S. Wang, Z. Chen, Y. Sun, Z. Gao, H. Zhang, J. Zhang, Electric-field-assisted growth of vertical graphene arrays and the application in thermal Interface materials, Adv. Funct. Mater. 30 (2020) 2003302, https://doi.org/10.1002/adfm.202003302.

[2] J.-D. Jhan, W.-Y. Teng, L.-Y. Hung, C. Chen, Y.-P. Wang, Advanced TIM material analysis for high performance package applications, 2024 International Conference on Electronics Packaging (ICEP), IEEE, Toyama, Japan, 2024, pp. 229–230, https://doi.org/10.23919/ICEP61562.2024.10535622.

[3] G. Chen, X. Xiao, X. Zhao, T. Tat, M. Bick, J. Chen, Electronic textiles for wearable point-of-care systems, Chem. Rev. 122 (2022) 3259–3291, https://doi.org/10.1021/acs.chemrev.1c00502.

[4] A. Libanori, G. Chen, X. Zhao, Y. Zhou, J. Chen, Smart textiles for personalized healthcare, Nat. Electron. 5 (2022) 142–156, https://doi.org/10.1038/s41928-022-00723-z.

[5] J. Xu, C. Duan, X. Wan, Z. Che, X. Zhao, Y. Zhou, Y. Song, J. Yin, T. Tat, S. Li, J. Chen, A soft magnetoelastic sensor to decode levels of fatigue, Nat. Electron. 8 (2025) 709–720, https://doi.org/10.1038/s41928-025-01418-x.

[6] X. Zhao, Y. Zhou, Y. Song, J. Xu, J. Li, T. Tat, G. Chen, S. Li, J. Chen, Permanent fluidic magnets for liquid bioelectronics, Nat. Mater. 23 (2024) 703–710, https://doi.org/10.1038/s41563-024-01802-6.

[7] Y. Zhou, X. Zhao, J. Xu, Y. Fang, G. Chen, Y. Song, S. Li, J. Chen, Giant magnetoelastic effect in soft systems for bioelectronics, Nat. Mater. 20 (2021) 1670–1676, https://doi.org/10.1038/s41563-021-01093-1.

[8] Z. Zhou, K. Chen, X. Li, S. Zhang, Y. Wu, Y. Zhou, K. Meng, C. Sun, Q. He, W. Fan, E. Fan, Z. Lin, X. Tan, W. Deng, J. Yang, J. Chen, Sign-to-speech translation using machine-learning-assisted stretchable sensor arrays, Nat. Electron. 3 (2020) 571–578, https://doi.org/10.1038/s41928-020-0428-6.

[9] X. Jia, S. Wang, S. Li, C. Xu, J. Du, J. Zhou, Z. Cheng, F. Zhou, Y. Deng, B. Liu, X. Huai, Anti-leak, self-adaptive liquid metal-epoxy in-situ cured composites with ultra-low thermal resistance via flexible droplet inclusions, Surf. Interfaces 42 (2023) 103335, https://doi.org/10.1016/j.surfin.2023.103335.

[10] B. Yang, J. Zeng, X. Luo, Z. Lin, M. Han, L. Ren, R. Sun, Y. Yao, Synergistic liquid metal-diamond-reinforced poly(ionic liquid) composites for high thermal conductivity and excellent reliability, ACS Appl. Mater. Interfaces 17 (2025) 32949–32962, https://doi.org/10.1021/acsami.5c07014.

[11] R. Cheng, Q. Wang, Z. Wang, L. Jing, A.V. Garcia-Caraveo, Z. Li, Y. Zhong, X. Liu, X. Luo, T. Huang, H.S. Yun, H. Salihoglu, L. Russell, N. Kazem, T. Chen, S. Shen, Liquid-infused nanostructured composite as a high-performance thermal interface material for effective cooling, Nat. Commun. 16 (2025) 794, https://doi.org/10.1038/s41467-025-56163-8.

[12] Z. Wang, J. Huang, W. Lin, R. Xu, C. Lin, Y. Lin, Surface-energy-matched interfaces as key design rule for ultra-low-resistance thermal interface materials, Adv. Funct. Mater. 36 (2026) e31931, https://doi.org/10.1002/adfm.202531931.

[13] H. Du, C. Xiao, M. Jiang, X. He, Y. Wang, X. Ding, X. Zhang, X. Li, K. Zheng, X. Liu, L. Chen, M. Xue, X. Tian, H. Zhang, Flexible polytetrafluoroethylene (PTFE) composite film with enhanced thermal conductivity and low interface thermal resistance for high frequency electronics, Polymer 285 (2023) 126367, https://doi.org/10.1016/j.polymer.2023.126367.

[14] J. Peng, J. Qian, T. Wei, Heat transfer performance of a novel graphene-based composite thermal interface material, J. Phys. Conf. Ser. 3112 (2025) 012090, https://doi.org/10.1088/1742-6596/3112/1/012090.

[15] L. Wang, J. Feng, H. Zhu, Y. Lv, Q. Yang, G. Li, M. Kong, Bottlebrush polysiloxane for designing high-loading thermal interface materials with excellent thermal conductivity efficiency and thixotropy, Compos. Part B Eng. 304 (2025) 112689, https://doi.org/10.1016/j.compositesb.2025.112689.

[16] L. Cai, J. Fan, S. Ding, D. He, X. Zeng, R. Sun, L. Ren, J. Xu, X. Zeng, Soft composite gels with high toughness and low thermal resistance through lengthening polymer strands and controlling filler, Adv. Funct. Mater. 33 (2023) 2207143, https://doi.org/10.1002/adfm.202207143.

[17] Q.-X. He, M.-M. Qin, H. Zhang, J. Yue, L. Peng, G. Liu, Y. Feng, W. Feng, Patterned liquid metal embedded in brush-shaped polymers for dynamic thermal management, Mater. Horiz. 11 (2023) 531–544, https://doi.org/10.1039/d3mh01498c.

[18] J. Li, Y. Pang, J. Wang, M. Yang, X. Zeng, L. Ren, R. Sun, Compliant composite elastomers via grafting short dangling chains for promoting thermal transport performance, Polym. Compos. 45 (2024) 12948–12958, https://doi.org/10.1002/pc.28679.

[19] H. Shi, W. Zhou, Z. Wen, W. Wang, X. Zeng, R. Sun, L. Ren, Thermally conductive and compliant polyurethane elastomer composites by constructing a tri-branched polymer network, Mater. Horiz. 10 (2023) 928–937, https://doi.org/10.1039/D2MH01140A.

[20] L. An, M. An, B. Yao, J. Song, X. Zhang, W. Ma, Unlocking the trade-off between intrinsic and interfacial thermal transport of boron nitride Nanosheets by surface functionalization for advanced thermal Interface materials, Adv. Mater. 37 (2025) 2412137, https://doi.org/10.1002/adma.202412137.

[21] J.W. Jang, I. Cha, J. Choi, J. Han, J.Y. Hwang, I.G. Cho, S.U. Son, E.J. Kang, C. Song, Biomass- and carbon dioxide-derived polyurethane networks for thermal Interface material applications, Polymers 16 (2024) 177, https://doi.org/10.3390/polym16020177.

[22] C. Guo, Y. Li, J. Xu, Q. Zhang, K. Wu, Q. Fu, A thermally conductive interface material with tremendous and reversible surface adhesion promises durable cross-interface heat conduction, Mater. Horiz. 9 (2022) 1690–1699, https://doi.org/10.1039/D2MH00276K.

[23] J. Lu, X. Ming, M. Cao, Y. Liu, B. Wang, H. Shi, Y. Hao, P. Zhang, K. Li, L. Wang, P. Li, W. Gao, S. Cai, B. Sun, Z.-Z. Yu, Z. Xu, C. Gao, Scalable compliant graphene Fiber-based thermal Interface material with metal-level thermal conductivity via dual-field synergistic alignment engineering, ACS Nano 18 (2024) 18560–18571, https://doi.org/10.1021/acsnano.4c04349.

[24] T. Xu, S. Zhou, F. Jiang, N. Song, L. Shi, P. Ding, Polyamide composites with improved thermal conductivity for effective thermal management: the three-dimensional vertically aligned carbon network, Compos. Part B Eng. 224 (2021) 109205, https://doi.org/10.1016/j.compositesb.2021.109205.

[25] H. Yu, L. Peng, C. Chen, M. Qin, W. Feng, Regulatable orthotropic 3D hybrid continuous carbon networks for efficient bi-directional thermal conduction, Nano Micro Lett. 16 (2024) 198, https://doi.org/10.1007/s40820-024-01426-0.

[26] Q. Liu, Y. Li, Z. Wu, J. Cheng, C. Jing, J. Cheng, J. Ma, J. Zhang, Record-high latent heat, ultra-fast relaxation and closed-loop recycling double-brush polymer networks for self-adaptive thermal Interface management, Adv. Sci. 13 (2026) e21482, https://doi.org/10.1002/advs.202521482.

[27] L.-M. Peng, Z. Xu, J. Yang, L. Bai, R.-Y. Bao, M.-B. Yang, W. Yang, Patternable thermal conductive interface materials enabled by vitrimeric phase change materials, Chem. Eng. J. 455 (2023) 140891, https://doi.org/10.1016/j.cej.2022.140891.

[28] D.D.L. Chung, Performance of thermal Interface materials, Small 18 (2022) 2200693, https://doi.org/10.1002/smll.202200693.

[29] Y. Wang, Z. Feng, M. Zhuang, J. Jiang, X. Jiang, Y. Yang, X. Li, K. Xi, Hyperbranched Polysiloxane-enhanced silicone elastomer composites for balanced thermal conductivity and mechanical properties in thermal Interface materials, ACS Appl. Mater. Interfaces 18 (2026) 2721–2735, https://doi.org/10.1021/acsami.5c21078.

[30] J. Fan, S. Ding, X. Zeng, S. Gao, Z. Wen, X. Zeng, R. Sun, L. Ren, Gecko-inspired adhesive structures enable efficiently thermal conductance and vibration dissipation in a highly mismatched system, Chem. Eng. J. 445 (2022) 136754, https://doi.org/10.1016/j.cej.2022.136754.

[31] J.-Y. Jeon, S.-J. Ha, H.-A. Cha, J.-H. Kim, C.-W. Ahn, J.-J. Choi, B.-D. Hahn, S.-H. Bae, Y.K. Moon, Engineering oxide ceramic fillers for thermal interface materials: enhanced thermal conductivity and thixotropy through hydrophobated

MgO/PDMS composite materials, Adv. Compos. Hybrid Mater. 8 (2025) 248, https://doi.org/10.1007/s42114-025-01316-y.
[32] M. Yang, Y. Pang, J. Li, W. Zhou, L. Ren, R. Sun, X. Zeng, Grafted alkene chains: triggers for defeating contact thermal resistance in composite elastomers, Small 20 (2024) 2305090, https://doi.org/10.1002/smll.202305090.
[33] L. Qiao, J. Zhou, F. Wang, Y. Gu, X. Ji, Y. Liu, Q. Ma, S. Cui, Y. Li, T. Yao, H. Yang, C. Wang, Biomimetic, viscoelastic and interface adaptive thermally conductive composites via lignin-induced supramolecular self-assembly for advanced thermal management, Adv. Compos. Hybrid Mater. 9 (2026) 55. doi:https://doi.org/10.1007/s42114-025-01589-3.
[34] J. Wang, T. Yang, Z. Wang, X. Sun, M. An, D. Liu, C. Zhao, G. Zhang, W. Lei, A Thermochromic, Viscoelastic Nacre-like Nanocomposite for the Smart Thermal Management of Planar Electronics, Nano-Micro Lett. 15 (2023) 170, https://doi.org/10.1007/s40820-023-01149-8.
[35] Z. Wu, J. Dong, H. Guo, R. Shang, X. Qin, Y. Xia, X. Li, X. Zhao, C. Ji, Q. Zhang, Robust, self-healing, and multi-use poly(urethane-urea-imide) elastomer as a durable adhesive for thermal Interface materials, Small 20 (2024) 2401815, https://doi.org/10.1002/smll.202401815.
[36] H. Zhang, Q. He, H. Yu, M. Qin, Y. Feng, W. Feng, A bioinspired polymer-based composite displaying both strong adhesion and anisotropic thermal conductivity, Adv. Funct. Mater. 33 (2023) 2211985, https://doi.org/10.1002/adfm.202211985.
[37] K. Huang, S. Pei, J. Guo, Q. Zhang, C. Ma, R. Liu, H.-M. Cheng, W. Ren, Surface-bulged graphene-lamellae networks with ultra-low thermal resistance, J. Mater. Sci. Technol. 236 (2025) 44–50, https://doi.org/10.1016/j.jmst.2025.03.009.
[38] P. Luo, Y. Tuersun, Y. Chen, Z. Chen, M. Li, Q. Huang, X. Chen, Z. Chen, S. Chu, Extremely low thermal resistance in solid-state thermal pad from in situ graphite cracking for high-power artificial intelligence chip, Matter 9 (2026) 102547, https://doi.org/10.1016/j.matt.2025.102547.
[39] Y. Wang, Y. Fan, K. Pan, Z. Liu, W. Zhao, X. Zhou, J. Qiu, Cocklebur-inspired robust non-flammable polymer Thermo conductor for CPU cooling, Small 21 (2025) 2405971, https://doi.org/10.1002/smll.202405971.
[40] Y. Xu, S. Wang, X. Sun, W. Han, Y. Li, Design and properties of graphene film/polymer square-wave-like composites, Chem. Eng. J. 507 (2025) 160215, https://doi.org/10.1016/j.cej.2025.160215.
[41] J. Zhu, N. Si, M. Wu, H. Zhang, Q. Li, B. Huang, H. Ma, T. Cai, Y. Wang, J. Yu, K. Wu, N. Jiang, C. Xue, W. Dai, X. Hu, C.-T. Lin, Q. Yan, Soft alumina-based thermal interface materials with enhanced thermal properties enabled by the synergistic effect with hexagonal boron nitride and liquid metal, J. Mater. Sci. Technol. 244 (2026) 60–69, https://doi.org/10.1016/j.jmst.2025.05.019.
[42] J.-Y. Koh, E. Choi, C. Lim, D. Kim, H.-K. Kim, S. Jang, A method for evaluating the cooling performance of a battery system assembly considering the mechanical behavior of the thermal interface material, J. Energy Storage 152 (2026) 120698, https://doi.org/10.1016/j.est.2026.120698.
[43] Y. Tuersun, X. Huang, M. Huang, W. Lin, P. Luo, H. Yang, S. Chu, Enhanced thermal performance from liquid metal in copper/graphite filled elastomer, J. Mater. Sci. Technol. 152 (2023) 247–255, https://doi.org/10.1016/j.jmst.2022.12.048.
[44] X. Teng, C. Ye, S. Zhang, Y. Zhu, Lamellar composites of vertical graphene and phase-change materials for highly efficient heat dissipation, ACS Nano 20 (2026) 2239–2247, https://doi.org/10.1021/acsnano.5c17391.
[45] Z. Huang, C. Wang, L. Zhou, C. Wu, Thermal conductivity enhancement and shape stability of phase-change materials using high-strength 3D graphene skeleton, Surf. Interfaces 26 (2021) 101338, https://doi.org/10.1016/j.surfin.2021.101338.
[46] H. Fenech, W.M. Rohsenow, Prediction of thermal conductance of metallic surfaces in contact, J. Heat Transfer 85 (1963) 15–24, https://doi.org/10.1115/1.3686003.
[47] D. Sun, E. You, T. Zhang, J. Xu, X. Wang, X. Ren, W. Tao, A review of thermal contact conductance research of conforming contact surfaces, Int. Commun. Heat Mass Transf. 159 (2024) 108065, https://doi.org/10.1016/j.icheatmasstransfer.2024.108065.
[48] D.D.L. Chung, Thermal Interface materials, J. Electron. Mater. 49 (2020) 268–270, https://doi.org/10.1007/s11664-019-07732-3.
[49] B. Wei, W. Luo, J. Du, Y. Ding, Y. Guo, G. Zhu, Y. Zhu, B. Li, Thermal interface materials: from fundamental research to applications, SusMat 4 (2024) e239, https://doi.org/10.1002/sus2.239.
[50] A.W. Shah, K. Wang, J.A. Siddique, W. Li, A comprehensive review of diamond-reinforced metal matrix composites for thermal management in high-performance electronics, J. Mater. Res. Technol. 33 (2024) 8174–8197, https://doi.org/10.1016/j.jmrt.2024.11.171.
[51] H. Niu, Y. Cao, K. Yang, H. Dong, Q. Cheng, Y. Chen, Review of boron nitride based polymer composites with ultrahigh thermal conductivity: critical strategies and applications, Compos. Part A Appl. Sci. Manuf. 200 (2026) 109289, https://doi.org/10.1016/j.compositesa.2025.109289.
[52] J. Wu, E. Zhou, A. Huang, H. Zhang, M. Hu, G. Qin, Deep-potential enabled multiscale simulation of gallium nitride devices on boron arsenide cooling substrates, Nat. Commun. 15 (2024) 2540, https://doi.org/10.1038/s41467-024-46806-7.
[53] Y. Cui, Z. Qin, H. Wu, M. Li, Y. Hu, Flexible thermal interface based on self-assembled boron arsenide for high-performance thermal management, Nat. Commun. 12 (2021) 1284, https://doi.org/10.1038/s41467-021-21531-7.
[54] Y. Ouyang, L. Qiu, X. Zhang, Y. Feng, Modulating heat transport inside CNT assemblies: multi-level optimization and structural synergy, Carbon 205 (2023) 236–252, https://doi.org/10.1016/j.carbon.2023.01.041.
[55] D.D.L. Chung, A critical review of carbon-based thermal interface materials, Mater. Chem. Phys. 309 (2023) 128432, https://doi.org/10.1016/j.matchemphys.2023.128432.
[56] J. Khan, S.A. Momin, M. Mariatti, A review on advanced carbon-based thermal interface materials for electronic devices, Carbon 168 (2020) 65–112, https://doi.org/10.1016/j.carbon.2020.06.012.
[57] D. Kuse, Y. Kaneko, R. Fujita, T. Horii, D. Shiojiri, Y. Ozawa, K. Nagatake, T. Takano, Y. Isoda, A. Koishikawa, T. Goto, A. Ueno, S. Maruo, K. Ueno, T. Fujie, H. Nagano, H. Ota, Nanolayer-encapsulated stretchable liquid-metal sheets for thermal management, Adv. Funct. Mater. 36 (2026) e27281, https://doi.org/10.1002/adfm.202527281.
[58] J.-W. Zhao, R. Zhao, Y.-K. Huo, W.-L. Cheng, Effects of surface roughness, temperature and pressure on interface thermal resistance of thermal interface materials, Int. J. Heat Mass Transf. 140 (2019) 705–716, https://doi.org/10.1016/j.ijheatmasstransfer.2019.06.045.
[59] R.S. Prasher, Rheology based modeling and design of particle laden polymeric thermal interface materials, in:, The Ninth Intersociety Conference on Thermal and Thermomechanical Phenomena In Electronic Systems (IEEE Cat. No.04CH37543),, 2004, pp. 36–44. Vol.1, https://doi.org/10.1109/ITHERM.2004.1319151.
[60] L. He, K. Wu, Q. Fu, Thermal conductivity modeling beyond the dilute limit using a body-centered cubic framework for densely packed polymer composites, Nat. Commun. 17 (2025) 327, https://doi.org/10.1038/s41467-025-67013-y.
[61] Z. Dou, C. Lei, K. Wu, G. Yu, The development of thermal interface materials, Nat. Electron. 8 (2025) 1146–1155, https://doi.org/10.1038/s41928-025-01543-7.
[62] Y. Guo, K. Ruan, X. Shi, X. Yang, J. Gu, Factors affecting thermal conductivities of the polymers and polymer composites: a review, Compos. Sci. Technol. 193 (2020) 108134, https://doi.org/10.1016/j.compscitech.2020.108134.
[63] Y. Ma, J. Fan, Y. Xiao, J. Wang, S. Cai, G. Lv, X. Xie, S. Cheng, S. Guo, L. Ren, J. Xu, R. Sun, X. Zeng, Fractal network design for soft, tough, antifatigue elastomer composites with high thermal conductivity, Compos. Part B Eng. 312 (2026) 113307, https://doi.org/10.1016/j.compositesb.2025.113307.
[64] S. Cai, J. Fan, J. Wang, Y. Ma, Y. Xiao, S. Cheng, G. Lv, X. Zeng, J. Xu, L. Ren, Y. Yao, X. Zeng, R. Sun, Yield-stress composite fluids with high thermal conductivity and tunable rheology via hierarchical filler architecture, Small 22 (2026) e13010, https://doi.org/10.1002/smll.202513010.
[65] Z. Xie, Z. Dou, D. Wu, X. Zeng, Y. Feng, Y. Tian, Q. Fu, K. Wu, Joint-inspired liquid and thermal conductive Interface for designing thermal Interface materials with high solid filling yet excellent Thixotropy, Adv. Funct. Mater. 33 (2023) 2214071, https://doi.org/10.1002/adfm.202214071.
[66] C.V. Madhusudana, Thermal contact conductance, springer international publishing, Cham, 2014, https://doi.org/10.1007/978-3-319-01276-6.
[67] J.A. Greenwood, J.B.P. Williamson, Contact of nominally flat surfaces, Proc. R. Soc. Lond. Ser. Math. Phys. Sci. 295 (1966) 300–319, https://doi.org/10.1098/rspa.1966.0242.
[68] R.I. Taylor, Rough surface contact modelling—a review, Lubricants 10 (2022) 98, https://doi.org/10.3390/lubricants10050098.
[69] M.G. Cooper, B.B. Mikic, M.M. Yovanovich, Thermal contact conductance, Int. J. Heat Mass Transf. 12 (1969) 279–300, https://doi.org/10.1016/0017-9310(69)90011-8.
[70] B.B. Mikić, Thermal contact conductance; theoretical considerations, Int. J. Heat Mass Transf. 17 (1974) 205–214, https://doi.org/10.1016/0017-9310(74)90082-9.
[71] R.S. Prasher, J.C. Matayabas, Thermal contact resistance of cured gel polymeric thermal Interface material, IEEE Trans. Compon. Packag. Technol. 27 (2004) 702–709, https://doi.org/10.1109/TCAPT.2004.838883.
[72] J. Zheng, Y. Li, L. Wang, H. Tan, An improved thermal contact resistance model for pressed contacts and its application analysis of bonded joints, Cryogenics 61 (2014) 133–142, https://doi.org/10.1016/j.cryogenics.2013.11.002.
[73] W. Zhou, W. Wang, H. Shi, X. Zeng, J. Li, Y. Pang, Y. Chang, R. Sun, L. Ren, Multiway softness polyurethane elastomeric composite with enhanced thermal conductivity and application as thermal Interface materials, Adv. Mater. Technol. 8 (2023) 2201701, https://doi.org/10.1002/admt.202201701.
[74] C.-K. Leong, D.D.L. Chung, Carbon black dispersions and carbon–silver combinations as thermal pastes that surpass commercial silver and ceramic pastes in providing high thermal contact conductance, Carbon 42 (2004) 2323–2327, https://doi.org/10.1016/j.carbon.2004.05.013.
[75] C. Lin, D.D.L. Chung, Nanoclay paste as a thermal Interface material for smooth surfaces, J. Electron. Mater. 37 (2008) 1698–1709, https://doi.org/10.1007/s11664-008-0538-9.
[76] A.M. Clausing, B.T. Chao, Thermal contact resistance in a vacuum environment, J. Heat Transfer 87 (1965) 243–250, https://doi.org/10.1115/1.3689082.
[77] A. Majumdar, C.L. Tien, Fractal network model for contact conductance, J. Heat Transfer 113 (1991) 516–525, https://doi.org/10.1115/1.2910594.
[78] W. Wu, J. Fan, C. Zeng, X. Cheng, X. Liu, S. Guo, R. Sun, L. Ren, Z. Hao, X. Zeng, Soft, tough, Antifatigue fracture elastomer composites with low thermal resistance through synergistic crack pinning and interfacial slippage, Adv. Mater. 36 (2024) 2403661, https://doi.org/10.1002/adma.202403661.
[79] X. Ge, R. Chen, J. Liu, M. Qu, Coating boron nitride Nanosheets with a Perfluoropolyether to improve thermal conductivity, ACS Appl. Nano Mater. 8 (2025) 5992–6003, https://doi.org/10.1021/acsanm.5c00104.
[80] Q. Hu, X. Bai, C. Zhang, X. Zeng, Z. Huang, J. Li, J. Li, Y. Zhang, Oriented BN/silicone rubber composite thermal interface materials with high out-of-plane thermal conductivity and flexibility, Compos. Part Appl. Sci. Manuf. 152 (2022) 106681, https://doi.org/10.1016/j.compositesa.2021.106681.

[81] X. Kong, Y. Chen, R. Yang, Y. Wang, Z. Zhang, M. Li, H. Chen, L. Li, P. Gong, J. Zhang, K. Xu, Y. Cao, T. Cai, Q. Yan, W. Dai, X. Wu, C.-T. Lin, K. Nishimura, Z. Pan, N. Jiang, J. Yu, Large-scale production of boron nitride nanosheets for flexible thermal interface materials with highly thermally conductive and low dielectric constant, Compos. Part B Eng. 271 (2024) 111164, https://doi.org/10.1016/j.compositesb.2023.111164.
[82] A. Bashir, H. Niu, M. Maqbool, A. Usman, R. Lv, Z. Ashraf, M. Cheng, S. Bai, A novel thermal Interface material composed of vertically aligned boron nitride and graphite films for ultrahigh through-plane thermal conductivity, Small Methods 8 (2024) 2301788, https://doi.org/10.1002/smtd.202301788.
[83] C.-P. Feng, J.-C. Ji, S.-C. Xu, L. Hou, G.-P. Cui, H.-B. Lan, F. Wei, J. Yang, W. Yang, Scalable thermal interface materials with close-packed structure and high through-plane thermal conductivity, Polym. Compos. 46 (2025) 10187–10196, https://doi.org/10.1002/pc.29613.
[84] Z. Lin, X. Luo, J. Zeng, T. Rao, Y. Jiang, L. Ren, R. Sun, Y. Yao, Engineering poly (ionic liquid) composites for silicone-free thermal Interface materials: enhanced thermal conductivity and interfacial adhesion, ACS Appl. Mater. Interfaces 17 (2025) 47543–47552, https://doi.org/10.1021/acsami.5c12774.
[85] S. Wang, J. Zhang, P. Yang, W. Zheng, R. Wang, R. Zhang, Y. Bai, L. Meng, S. Sun, Thermal Interface materials with excellent flexibility and adhesion via chain segment structure design, Polym. Compos. 47 (2026) 231–240, https://doi.org/10.1002/pc.70140.
[86] X. Luo, Z. Lin, B. Yang, T. Rao, J. Zeng, Y. Jiang, L. Ren, R. Sun, Y. Yao, Poly(ionic liquid)-based thermal Interface materials with enhanced interfacial adhesion and thermal stability for advanced electronic cooling, Adv. Mater. Technol. 10 (2025) e01321, https://doi.org/10.1002/admt.202501321.
[87] S. Ding, D. He, L. Cai, X. Zeng, X. Zeng, L. Ren, G. Du, J. Fan, Optimizing thermal properties of thermal Interface materials using the adhesion mechanism of gecko's setae, IEEE, Dalian, China, 2022, pp. 1–5, https://doi.org/10.1109/ICEPT56209.2022.9872543, 23rd International Conference on Electronic Packaging Technology (ICEPT),., 2022, pp.
[88] I. Cha, T. Kim, K.-S. Kim, S. Baik, C. Song, Ultralow contact resistance of thermal Interface materials enabled by the Vitrimer chemistry of a β-Hydroxy phosphate Ester, Chem. Mater. 35 (2023) 7491–7499, https://doi.org/10.1021/acs.chemmater.3c00995.
[89] Y. Ji, Z. Wen, J. Fan, X. Zeng, X. Zeng, R. Sun, L. Ren, Adaptable thermal conductive, high toughness and compliant poly(dimethylsiloxane) elastomer composites based on interfacial coordination bonds, Compos. Sci. Technol. 231 (2023) 109840, https://doi.org/10.1016/j.compscitech.2022.109840.
[90] C. Liu, W. Yu, J. Fan, Y. Li, J. Chen, J. Fu, G. Peng, J. Liu, Open package form-stable phase change microspheres with low thermal contact resistance for the thermal management of electronic devices, Appl. Therm. Eng. 241 (2024) 122396, https://doi.org/10.1016/j.applthermaleng.2024.122396.
[91] R. Bai, Y. Wei, J. Xu, X. Li, M. Li, Z. Zou, X. Huang, C. Liu, Y. Sun, M. Hao, Encapsulated carbon nanotube array as a thermal interface material compatible with standard electronics packaging, Nano Res. 16 (2023) 11389–11400, https://doi.org/10.1007/s12274-023-5872-y.
[92] H. Huang, C. Wang, T. Wu, Z. Wu, J. Zheng, Phase change thermal interface materials with interface adaptability and self-healing properties, Surf. Interfaces 55 (2024) 105406, https://doi.org/10.1016/j.surfin.2024.105406.
[93] K. Ou, Y. Pang, M. Yang, Y. Wei, X. Xie, X. Zeng, L. Zhang, X. Zeng, C. Li, R. Sun, Phase-change composite elastomers for efficient thermal management at contact interface, Compos. Commun. 52 (2024) 102149, https://doi.org/10.1016/j.coco.2024.102149.
[94] Z. Ye, C. Ji, T. Yu, R. Sun, X. Zeng, B. Cao, Enhanced interfacial heat-transfer of Al2O3-MXene-silicone composite via an electrostatic self-assembly strategy, Int. J. Heat Mass Transf. 199 (2022) 123430, https://doi.org/10.1016/j.ijheatmasstransfer.2022.123430.
[95] S. Song, S. Zhao, X. Wang, Q. Liang, J. Li, X. Zhang, Y. Li, Enhancement of thermal performance of composite phase change materials by graphite in situ modified Al_2O_3 porous support, ACS Appl. Polym. Mater. 5 (2023) 7350–7357, https://doi.org/10.1021/acsapm.3c01261.
[96] T. Kim, S. Kim, E. Kim, T. Kim, J. Cho, C. Song, S. Baik, High-temperature skin softening materials overcoming the trade-off between thermal conductivity and thermal contact resistance, Small 17 (2021) 2102128, https://doi.org/10.1002/smll.202102128.
[97] R.-Y. Bao, L.-M. Peng, J. Yang, L. Bai, M.-B. Yang, W. Yang, Vitrimeric phase change material facilitating 3D-structured boron nitride network for reliable thermal conductive interface materials, Polymer 299 (2024) 126989, https://doi.org/10.1016/j.polymer.2024.126989.
[98] M. Alayli, T. Kim, S. Cheon, S. Baik, Significantly enhanced conformal contact by the functional layers on a copper film for thermal Interface materials, Adv. Eng. Mater. 26 (2024) 2301823, https://doi.org/10.1002/adem.202301823.
[99] Y. Huang, W. Luo, W. Chen, X. Hu, G. Zhu, Y. Ma, X. Jiang, Q. Li, Self-healing, adaptive and shape memory polymer-based thermal interface phase change materials via boron ester cross-linking, Chem. Eng. J. 496 (2024) 153789, https://doi.org/10.1016/j.cej.2024.153789.
[100] L. Sun, Y. Huang, W. Chen, X. Jiang, X. Hu, Chemically crosslinked flexible polymer phase change material with self-healing, self-adaptive, and shape-memory properties for thermal interface applications, J. Colloid Interface Sci. 695 (2025) 137831, https://doi.org/10.1016/j.jcis.2025.137831.
[101] X. Chen, L. Fan, X. Guo, H. Zheng, S. Cheng, P. Zheng, L. Zheng, X. Zhang, Y. Zhang, Self-adaptive thermal interface materials featuring low thermal resistance by combining phase change materials with magnetic field-induced filler alignment, Compos. Part B Eng. 304 (2025) 112687, https://doi.org/10.1016/j.compositesb.2025.112687.
[102] Q. Lu, X. Wang, H. Zhao, X. Wang, J. Zhao, H. Kong, T. Wang, C. Liang, J. Li, W. Q. Xu, A hierarchically encapsulated phase-change film with multi-stage heat management properties and conformable self-interfacing contacts for enhanced interface heat dissipation, J. Mater. Chem. A 10 (2022) 23617–23629, https://doi.org/10.1039/D2TA05582A.
[103] D. Li, C. Ding, S. Shen, J. Wang, L. Wu, B. You, G. Tao, Mussel-mimetic thermal conductive films with solid-solid phase change and shape-adaptive performance, J. Mater. Chem. A 12 (2024) 11511–11523, https://doi.org/10.1039/d4ta00031e.
[104] C. Liu, J. Yang, Y. Li, J. Fu, W. Yu, H. Xie, BN green gel thermal interface material with high thermal conductivity and low thermal contact resistance for efficiently thermal management, Surf. Interfaces 47 (2024) 104204, https://doi.org/10.1016/j.surfin.2024.104204.
[105] Z.Y. Jiang, J.Y. Li, Z.G. Qu, L. Wang, J.Y. Miao, Theoretical analysis on thermal grease dry-out degradation in space environment, Int. J. Therm. Sci. 179 (2022) 107694, https://doi.org/10.1016/j.ijthermalsci.2022.107694.
[106] X. Jia, B. Liu, S. Li, X. Li, J. Zhou, G. Zhou, S. Wang, M. Xu, C. Xu, J. Du, Y. Deng, X. Huai, High-performance non-silicone thermal interface materials based on tunable size and polymorphic liquid metal inclusions, J. Mater. Sci. 57 (2022) 11026–11045, https://doi.org/10.1007/s10853-022-07210-y.
[107] P. Luo, Y. Tuersun, X. Huang, H. Yang, S. Chu, Study of the mechanism of liquid-metal-assisted thermal Interface materials, Adv. Eng. Mater. 25 (2023) 2301092, https://doi.org/10.1002/adem.202301092.
[108] K. Wu, Z. Dou, S. Deng, D. Wu, B. Zhang, H. Yang, R. Li, C. Lei, Y. Zhang, Q. Fu, G. Yu, Mechanochemistry-mediated colloidal liquid metals for electronic device cooling at kilowatt levels, Nat. Nanotechnol. 20 (2025) 104–111, https://doi.org/10.1038/s41565-024-01793-0.
[109] W. Dai, X.-J. Ren, Q. Yan, S. Wang, M. Yang, L. Lv, J. Ying, L. Chen, P. Tao, L. Sun, C. Xue, J. Yu, C. Song, K. Nishimura, N. Jiang, C.-T. Lin, Ultralow interfacial thermal resistance of graphene thermal Interface materials with surface metal liquefaction, Nano Micro Lett. 15 (2022) 9, https://doi.org/10.1007/s40820-022-00979-2.
[110] X. Zhang, Y. Dong, Y. Du, L. Yang, W. Ma, B. Cao, Improving the thermal performance of liquid metal thermal interface materials: the role of intermetallic compounds at the gallium/copper interface, Adv. Mater. Interfaces 12 (2025) 2500041, https://doi.org/10.1002/admi.202500041.
[111] H. Kuang, H. Bai, C. Yuan, F. Guo, Z. Zheng, Y. Zhao, Z. Wang, C. Yu, J. Zhang, Enhancing wettability and reducing thermal contact resistance of liquid metal–graphene film interfaces via metal coating modification, Appl. Therm. Eng. 288 (2026) 129702, https://doi.org/10.1016/j.applthermaleng.2026.129702.
[112] X. Wang, Y. Wang, B. Yang, Y. Guo, K. Xu, Z. Zhang, R. Yang, J. Zhang, B. Zhu, Y. Qin, Y. Zhou, L. Li, M. Li, T. Cai, K. Nishimura, C.-T. Lin, N. Jiang, W. Dai, J. Yu, Morphology-controllable liquid metal/diamond Sandwich-structured thermal Interface material toward high-efficiency thermal management, ACS Nano 19 (2025) 20956–20969, https://doi.org/10.1021/acsnano.5c03918.
[113] A. Aiyiti, X. Bai, J. Wu, X. Xu, B. Li, Measuring the thermal conductivity and interfacial thermal resistance of suspended MoS2 using electron beam self-heating technique, Sci. Bull. 63 (2018) 452–458, https://doi.org/10.1016/j.scib.2018.02.022.
[114] D. Ren, F. Zhang, Y. Sun, D. Liu, Q. Zheng, Silicon carbide-welded boron nitride networks for self-healing flexible thermal Interface materials, ACS Appl. Mater. Interfaces 17 (2025) 61280–61291, https://doi.org/10.1021/acsami.5c16186.
[115] J. Zeng, X. Li, T. Liang, T. Rao, Z. Zheng, Y. Yao, J.-B. Xu, R. Sun, L. Li, Thermally conductive and self-healable liquid metal elastomer composites based on poly (ionic liquid)s, Compos. Part A Appl. Sci. Manuf. 194 (2025) 108922, https://doi.org/10.1016/j.compositesa.2025.108922.
[116] L. Jing, R. Cheng, M. Tasoglu, Z. Wang, Q. Wang, H. Zhai, S. Shen, T. Cohen-Karni, R. Garg, I. Lee, High thermal conductivity of Sandwich-structured flexible thermal Interface materials, Small 19 (2023) 2207015, https://doi.org/10.1002/smll.202207015.
[117] Y. Tuersun, W. Lin, X. Huang, W. Qiu, P. Luo, M. Huang, S. Chu, Fabrication and pilot-production of ultrahigh thermal conductivity vertical graphite-silicone pads with very low cost, Carbon 194 (2022) 72–80, https://doi.org/10.1016/j.carbon.2022.03.053.
[118] T. Okumura, T. Nakano, Y. Inoue, Film-type carbon nanotube thermal interface materials for advanced thermal management: a study on interfacial resistance, Carbon 250 (2026) 121288, https://doi.org/10.1016/j.carbon.2026.121288.
[119] R. Yang, Y. Wang, Z. Zhang, K. Xu, L. Li, Y. Cao, M. Li, J. Zhang, Y. Qin, B. Zhu, Y. Guo, Y. Zhou, T. Cai, C.-T. Lin, K. Nishimura, C. Xue, N. Jiang, J. Yu, Highly oriented BN-based TIMs with high through-plane thermal conductivity and low compression modulus, Mater. Horiz. 11 (2024) 4064–4074, https://doi.org/10.1039/d4mh00626g.
[120] K. Zhan, Y. Chen, Z. Xiong, Y. Zhang, S. Ding, F. Zhen, Z. Liu, Q. Wei, M. Liu, B. Sun, H.-M. Cheng, L. Qiu, Low thermal contact resistance boron nitride nanosheets composites enabled by interfacial arc-like phonon bridge, Nat. Commun. 15 (2024) 2905, https://doi.org/10.1038/s41467-024-47147-1.
[121] Q. Liang, X. Yao, W. Wang, Y. Liu, C.P. Wong, A three-dimensional vertically aligned functionalized multilayer graphene architecture: An approach for graphene-based thermal interfacial materials, ACS Nano 5 (2011) 2392–2401, https://doi.org/10.1021/nn200181e.
[122] K. Hayashi, T. Nakano, Y. Inoue, Enhancing thermal conduction properties of vertically aligned CNT forests by reducing interfacial thermal resistance using an aluminum interlayer, Carbon 238 (2025) 120256, https://doi.org/10.1016/j.carbon.2025.120256.
[123] H. Fu, R. Fang, C. Tian, W. Qian, S. Cao, Z. Zhang, X. Xu, C. Yao, Z. Wang, D. He, High-performance thermal interface materials enabled by vertical alignment of

lightweight and soft graphene foams, Nano Res. 17 (2024) 9293–9299, https://doi.org/10.1007/s12274-024-6985-7.
[124] S. Li, Y. Li, Z. Yi, L. Xie, W. Li, H. Jia, F. Su, High-throughput screening enables ultrathin and high thermal conductivity all-carbon graphene foam thermal Interface materials, Small 22 (2026) e12639, https://doi.org/10.1002/smll.202512639.
[125] W. Dai, T. Ma, Q. Yan, J. Gao, X. Tan, L. Lv, H. Hou, Q. Wei, J. Yu, J. Wu, Y. Yao, S. Du, R. Sun, N. Jiang, Y. Wang, J. Kong, C. Wong, S. Maruyama, C.-T. Lin, Metal-level thermally conductive yet soft graphene thermal Interface materials, ACS Nano 13 (2019) 11561–11571, https://doi.org/10.1021/acsnano.9b05163.
[126] T. Huang, T. Wang, J. Jin, M. Chen, L. Wu, Design of Silicon Rubber/BN film with high through-plane thermal conductivity and ultra-low contact resistance, Chem. Eng. J. 469 (2023) 143874, https://doi.org/10.1016/j.cej.2023.143874.
[127] C. Tian, H. Fu, Z. Wang, Z. Zhang, W. Qian, H. Zhang, S. Xu, S. Cao, D. He, Deformable surface design of vertical graphene thermal interface materials for efficient heat dissipation, Cell Rep. Phys. Sci. 5 (2024) 101978, https://doi.org/10.1016/j.xcrp.2024.101978.
[128] Q. He, H. Zhang, Z. Zhang, Y. Duan, M. Qin, W. Feng, Dandelion-inspired radial oriented microspheres for dynamic interface thermal management, Adv. Funct. Mater. 36 (2026) e20631, https://doi.org/10.1002/adfm.202520631.
[129] S. Chen, Y. Guo, Q. Pan, Y. Shuai, A review on current development of thermophotovoltaic technology in heat recovery, Int. J. Extreme Manuf. 6 (2024) 022009, https://doi.org/10.1088/2631-7990/ad1dca.
[130] Z.-Q. Yu, M.-T. Li, B.-Y. Cao, A comprehensive review on microchannel heat sinks for electronics cooling, Int. J. Extreme Manuf. 6 (2024) 022005, https://doi.org/10.1088/2631-7990/ad12d4.
[131] X. Zhang, X. Yang, Y. Fan, R. Hu, B. Xie, X. Luo, 3D-programmable streamline guided orientation in composite materials for targeted heat dissipation, Int. J. Extreme Manuf. 7 (2025) 025504, https://doi.org/10.1088/2631-7990/ad92cb.
[132] S. Zhong, B. Lu, D. Wang, B. Arianpour, S. Wang, H. Han, J. Yin, H. Bao, Y. Liu, Z. Wen, Y. Zhou, Passive isothermal flexible sensor enabled by smart thermal-regulating aerogels, Adv. Mater. 37 (2025) 2415386, https://doi.org/10.1002/adma.202415386.